Heartbeat Detection using Infrared Thermometry in the Ear

D. K. Kuratomi

Heartbeat Detection using Infrared Thermometry in the Ear

by

D. K. Kuratomi

to obtain the degree of Master of Science in Biomedical Engineering
at the Delft University of Technology,
to be defended publicly on August 30, 2017 at 14:00.

Student number:	4521544	
Project duration:	November 14, 2016 – August 10, 2017	
Thesis committee:	Dr. G. de Graaf,	TU Delft, Daily supervisor
	Prof. dr. P.J. French,	TU Delft, Supervisor
	Dr. G. Pandraud,	TU Delft
	Dr. ir. J.C. Haartsen,	Plantronics

An electronic version of this thesis is available at `http://repository.tudelft.nl/`.

TU Delft

Abstract

Heart rate is a key factor in cardiovascular system monitoring and sports science. Some recent commercial applications use sensors in the ear but are faced with motion artifacts which corrupts the signal. In this report, a comprehensive review of heart rate detection methodologies was completed in order to find possible solutions with better performance. Infrared thermography is a non-contact technique and was selected because it may minimize motion effects with better user comfort and lower power consumption.

Thermopiles were chosen as the sensors used in the system based on their responsivity, relevant wavelength detection and size. The anatomical distribution of the arteries in the external ear was studied in order to select the best position of the sensor. The cavum conchae and anti-tragus were studied considering the irrigation of the posterior auricular and superficial temporal arteries. The signal analysis was performed using a continuous wavelet transform which extract frequency features of the bioheat transfer waveforms.

A digital sensor was evaluated first in the neck, nose, wrist and ear but did not render relevant results mainly due to quantization errors. Subsequently, analog thermopiles were studied with ultra-low noise amplifiers. First, the Noise Equivalent Temperature Difference from a ST150 thermopile was calculated using a Peltier cooler and a Pt100 reference sensor. This sensor was then used to measure the infrared signals of the wrist, neck and ear in order to find pertinent heart rate signal.

Next, a smaller sensor ZTP-135SR was used to try compare the locations of the anti-tragus and the cavum conchae in the ear and under the effect of a fan. The fan did not had any effect on the measurement and the smaller sensor had significantly less signal than the previous sensor. The localization of the arteries was not possible as a result of the reduction on the detection area of the skin. Finally, the effect of the detection area of the skin was tested under 2 conditions using the ST150 thermopile. The results show that a separation of the sensor from the skin increased the detection area and the quality of the heart rate signal measured. The proposed system successfully uses infrared differential thermometry to detect the heart rate in the auricle.

Acknowledgments

This project has been produced with the cooperation between Plantronics and the Delft University of Technology and it would not have been possible without the help and support of many people. I would like to start thanking my supervisors Dr. Ger de Graaf and Prof. dr. P.J. French for all the support and technical advice I received during the execution of this project.

I also want to express my gratitude to Dr. ir. J.C. Haartsen and F. Hooijschuur that mentored me and taught me numerous valuable things during my stay in Emmen and during the execution of the project. Finally, I want to thank my family and friends for all their support with a special mention to Alejandra whose love and encouragement was invaluable to me.

Contents

List of Figures vi

1 Introduction 1

2 Background 3
2.1 Current Products and Prototypes . . . 3
2.2 Motion Artifacts . . . 4
2.3 State of the Art . . . 5
2.3.1 Electrical Methods . . . 5
2.3.2 Mechanical Methods . . . 7
2.3.3 Thermal Methods . . . 8
2.3.4 Radiant Methods . . . 9
2.4 Comparison and Selection . . . 11
2.5 Bioheat Transfer . . . 13
2.6 Ear Anatomy . . . 15
2.6.1 Tissue composition . . . 15
2.6.2 Blood irrigation . . . 15
2.7 The Wearable Issue . . . 16
2.8 Requirements . . . 16

3 System Design 18
3.1 Ear Location . . . 18
3.2 Infrared Sensor . . . 19
3.3 Signal Processing . . . 21

4 Experimental Designs 23
4.1 Digital sensor . . . 23
4.2 Noise Equivalent Temperature Difference (NETD) . . . 24
4.3 Proof of concept test . . . 26
4.4 Arterial irrigation test . . . 27
4.5 Area of measurement test . . . 27

5 Results 28
5.1 Digital sensor . . . 28
5.2 Noise Equivalent Temperature Difference . . . 31
5.3 Proof of concept test . . . 32
5.4 Arterial irrigation test . . . 35
5.5 TO-5 Size . . . 42

6 Conclusion 46

A Appendix 48
A.1 ECG front end used . . . 48

A.2 Low Noise Amplifier 49
A.3 Filter 49
A.4 Signal Acquisition 50
A.5 PCB Layout 50

B Appendix **53**
B.1 MATLAB Code 53

Bibliography **56**

List of Figures

1.1 Training zones based on heart rate developed by Fox and Haskell 2

2.1 Available HR products in the market with their corresponding release date . . 3
2.2 Physical domain and methodologies of heart rate detection 4
2.3 Example of the effects of motion artifacts in a PPG signal 5
2.4 Cardiac events and resulting ECG and PCG signals 6
2.5 Example of a finger-based pulse oximeter 10
2.6 Summary of all heart rate detection methods covered 11
2.7 Comparison of all the HR measurement methods 13
2.8 Tissue layers that separate the blood flow from the environment 14
2.9 Names of the auricle parts 15
2.10 Blood vessels located near the inner ear [44] 16

3.1 A) Distribution of arteries in the external ear. The green circle signals the antitragus and the blue circle signals the cavum conchae. B) Earpieces with corresponding modifications of the positioning of the sensors 18
3.2 Atmospheric transmission of IR signals. The second atmospheric window contains the radiation of the human skin 19
3.3 Size comparison of an earpiece, a 2 Euro coin, a TO5 sensor and a TO46 sensor 21
3.4 Different types of wavelets available for CWT 22

4.1 Block diagram of the system used to take measurements with the digital sensor 23
4.2 Diagram of the set-up of the thermopile, the Pt100 temperature sensor and the peltier cooler 25
4.3 Block diagram of the system used to take measurements to find the NETD of the sensor at ambient temperature 25
4.4 Location of the thermopile in the ear and electrodes used for the measurements of infrared thermometry and ECG 26
4.5 Block diagram of the system implemented to take the first measurements of the thermopile ST150 26
4.6 Block diagram of the system implemented to take the low noise measurements using the analog thermopiles 27

5.1 Excerpt of the output of the Digital sensor and corresponding ECG signal of a sample in the ear 28
5.2 Contour plot of CWT coefficients of the ECG signal and the digital infrared signal from a sample in the ear 29
5.3 Heart rate detected from the digital sensor signal (Orange) and ECG signal (Blue) from a sample in the ear 30
5.4 Contour plot of CWT coefficients of the ECG signal and the digital infrared signal from a sample in the neck 30

5.5 Linear regression of the Responsivity of the ST150 sensor 32
5.6 Behavior of the signal output of the ST150 at 0.5, 2 and 4 Hz 33
5.7 Excerpt of the output of the ST150 and corresponding ECG signal of a sample in the neck 33
5.8 Contour plot of CWT coefficients of the ECG signal and the ST150 signal from a sample in the neck 34
5.9 Heart rate detected from the ST150 sensor signal (Orange) and ECG signal (Blue) from a sample in the neck 34
5.10 Contour plot of CWT coefficients of the ECG signal and the ST150 signal from a sample in the ear 35
5.11 Heart rate detected from the ST150 signal (Orange) and ECG signal (Blue) from a sample in the ear 36
5.12 Boxplot of the correlation percentages based on the location with a 3.5 BPM range for the ST150 37
5.13 Boxplot of the correlation percentages based on the location with a 10.5 BPM range for the ST150 37
5.14 Excerpt of the output of the ZTP-135SR and corresponding ECG signal of a sample in the ear 38
5.15 Contour plot of CWT coefficients of the ECG signal and the ZTP-135SR signal from a sample in the ear 39
5.16 Heart rate detected from the ZTP-135SR signal (Orange) and ECG signal (Blue) from a sample in the ear 39
5.17 Boxplot of the correlation percentages based on the 4 treatments with a 3.5 BPM range for the ZTP-135SR 40
5.18 Boxplot of the correlation percentages based on the 4 treatments with a 10.5 BPM range for the ZTP-135SR 40
5.19 Boxplot of the correlation percentages based only on the location with a 3.5 BPM range for the ZTP-135SR 41
5.20 Boxplot of the correlation percentages based only on the location with a 10.5 BPM range for the ZTP-135SR 41
5.21 Excerpt of the output of the ST150 and corresponding ECG signal of a sample in the ear at 1 cm separation 42
5.22 Contour plot of CWT coefficients of the ECG signal and the ST150 signal from a sample in the ear at 1 cm separation 43
5.23 Heart rate detected from the ST150 signal (Orange) and ECG signal (Blue) from a sample in the ear at 1 cm separation 43
5.24 Boxplot of the correlation percentages based on the separation distance with a 3.5 BPM range for the ST150 44
5.25 Boxplot of the correlation percentages based on the separation distance with a 10.5 BPM range for the ST150 44
5.26 Boxplot of the correlation percentages based only ear measurements with a 3.5 BPM range for all sensors 45
5.27 Boxplot of the correlation percentages based only ear measurements with a 10.5 BPM range for all sensors 45

A.1 ECG front-end module used for control measurements 48
A.2 Standard PQRST complex waveform 49

A.3 NI USB 6210 used to acquire the analog signals from the ECG and the IR sensor 50
A.4 Circuit Diagram of the complete board 51
A.5 Front side of the PCB 52
A.6 Back layer of the PCB 52
A.7 The shielded system connected with the input (blue coaxial cable) and the ECG module (black cable) 52

1 Introduction

Heart rate (HR) is one of the vital signs that can be gathered from a person along with temperature, respiration rate and blood pressure. It gives essential information about the state of the cardiovascular system and can be used to identified several pathologies. Heart rate is defined as the amount of heart pulses in a set unit of time, it is usually presented in beats per minute (BPM). It is used in many different scenarios ranging from a hospital bed to the training grounds for Olympic athletes. The measurement of the heart rate its done in emergencies to detect irregular pulses known as Arrhythmia, low heart rate (Bradycardia) and high heart rate (Tachycardia) [42]. It is also measured in care units to detect changes in the patients health status to react faster to crises.

In sports science, the HR is commonly used as an approximation of a calorimetry reading. Calorimetry is the measurement of the energy consumption of a person and it is taken as the maximum oxygen uptake a person can use in a time interval (Also known as VO2Max). This type of measurement requires a specialized laboratory to quantify the oxygen intake of a person during a specific training on a treadmill or a stationary bike. With the information about the maximum physical performance of a person, the range between resting and maximum energy consumption is divided into zones. Several theories regarding this training zones were developed to separate training intensities, a linear relation is often used between the HR and the VO2Max [34]. Figure 1.1 shows an example of zones divided according to the percentage of maximum HR, this relation is used to generate coaching plans using only the HR by many products in the market [32].

Heart rate is also used as a marker for stress and disease analysis which can be useful in different locations such as offices and airports, it can be used to see the stress of workers and prevent injuries in an office setting and can also be used to detect stress levels in planes and military training. There is also a lot of developments trying to measure heart rate to detect when drivers fall asleep behind the wheel [7]. There are also other factors that affect heart rate such as caffeine and lack of sleep that increase the BPM.

The time between the heart beats is not constant, the separation between the beats can have small variations that are currently being associated to different cardiovascular complications. Some research teams argue that these variations are a signal of the current state

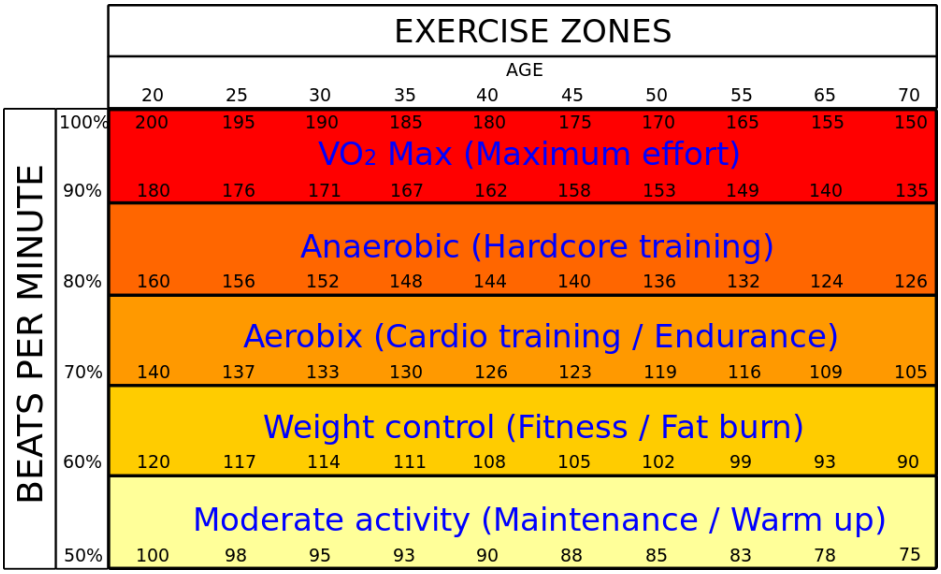

Figure 1.1: Training zones based on heart rate developed by Fox and Haskell

of the cardiac system and that an increase in variation can preemptively signal the occurrence of cardiac complications. This new measurement requires a much more precise peak detection method, since a normal HR detection method only requires to know if a peak occurred rather the exact time it happened [38].

Long term heart rate measurements require devices that maximize user comfort with high portability that do not restrict user movement. Several approaches have been implemented in the last decades with the most common technology used being photoplethysmography (PPG) sensors in wearable devices [28]. This project aimed to design and implement a system that is capable of detecting heart beats on an earpiece. In the second chapter, all the developed heart rate detection methodologies available in literature are explored and the most suitable to be implemented in an earpiece was selected. Chapter 3 describes the most important concepts for heart beat detection in the ear including location, sensor selection and signal extraction. Chapter 4 defines the experimental designs used to evaluate the implemented systems and chapter 5 presents all the results obtained. Finally, the conclusions are presented in chapter 6.

2

Background

2.1. Current Products and Prototypes

The leading brand for sports heart rate measurement is Polar from Finland. With over 40 years in the market, their solution is always used as a robust solution. They combine the chest ECG measurement with the first smartwatches to provide the HR signal. Figure 2.1 shows some examples and release dates of products in different categories.

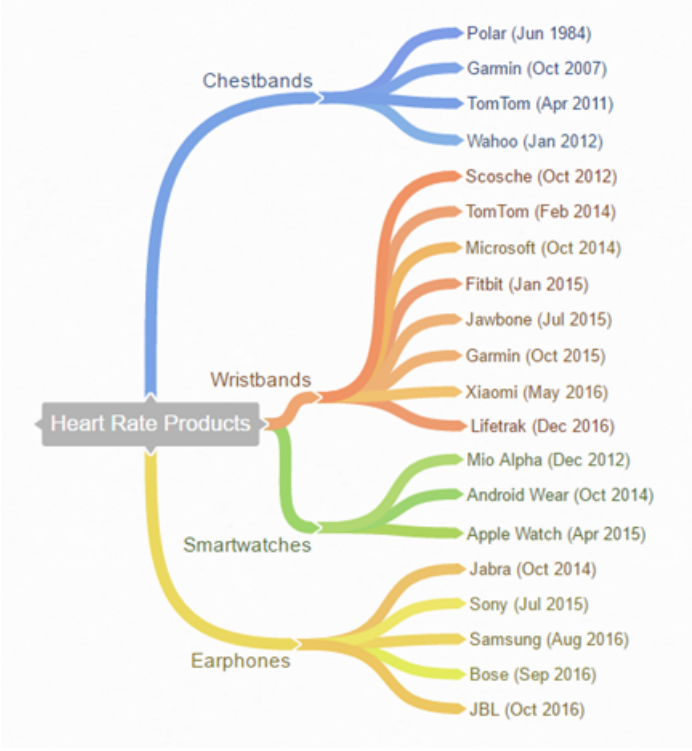

Figure 2.1: Available HR products in the market with their corresponding release date

The sportsbands were the second wave of health oriented wearables. The main brands available are the jawbone and the Fitbit that were followed by the integration of health sensors in the smartwatches of Samsung, Google and Apple. Other brands available include

Nike, Misfit and Bowflex. The sportswatchs usually integrate an accelerometer sensor to detect the number of steps and general physical activity made by the user per day. Most of the sportsband and smartwatches available that detect heart rate use green PPG technology excluding a Jawbone model that uses ICG measurement.

Currently there are several earphone brands that offer heart rate measurement. One of the first brands to develop this product was Jabra that was followed by Bose and Samsung. Other brands like Underarmour (UA) and Sony also have products available. Jabra implements sensors from US-based company Valencell.

To classify the different heart rate measurements methods available, different domains were specified based on the nature of the phenomena measured. Figure 2.2 shows each of the domain studied and the different methods that will be covered in the next sections.

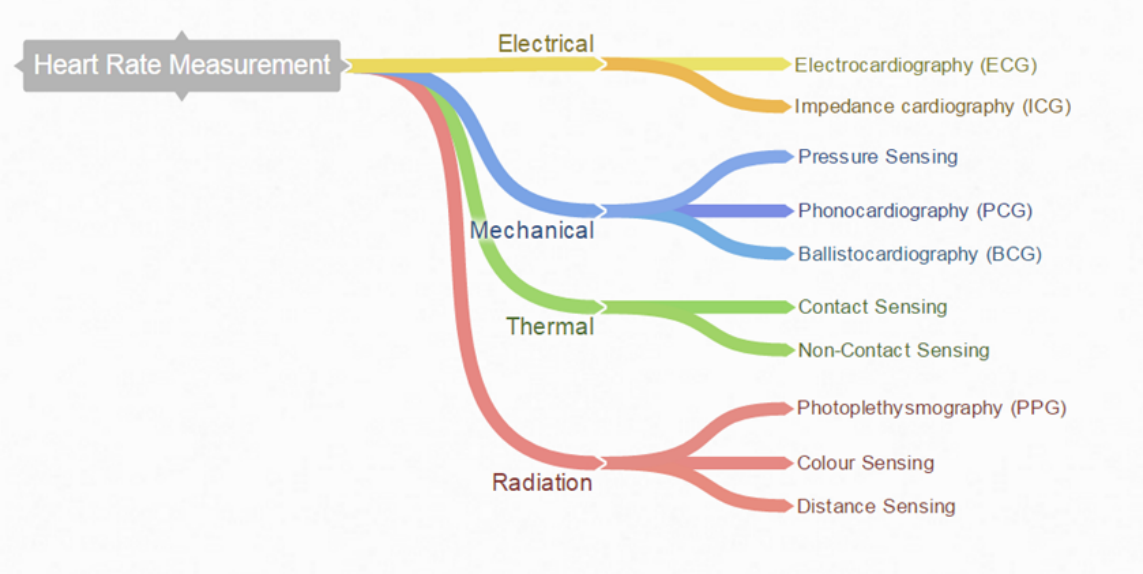

Figure 2.2: Physical domain and methodologies of heart rate detection

2.2. Motion Artifacts

Before presenting the different technologies, it is important to understand what is the main problem that affects current heart rate measurements. Motion artifacts are a corruption of the heart signals due to movement effects. These effects can have different sources depending on the measurement method being used. Still, the effect is undesirable in virtually all the current heart rate extraction methods. For instance, medical applications require high resolution measurements which can be affected even by breathing movement while sports applications are affected by strong user movement.

In the case of Photoplethysmography, the noise is caused by the separation of the skin and the sensor. The movement of the sensor increases and reduces the distance from the skin as the sensor moves at a different time than the body due to inertial differences. The separation changes the light refraction and it changes the signal as if the tissue measured

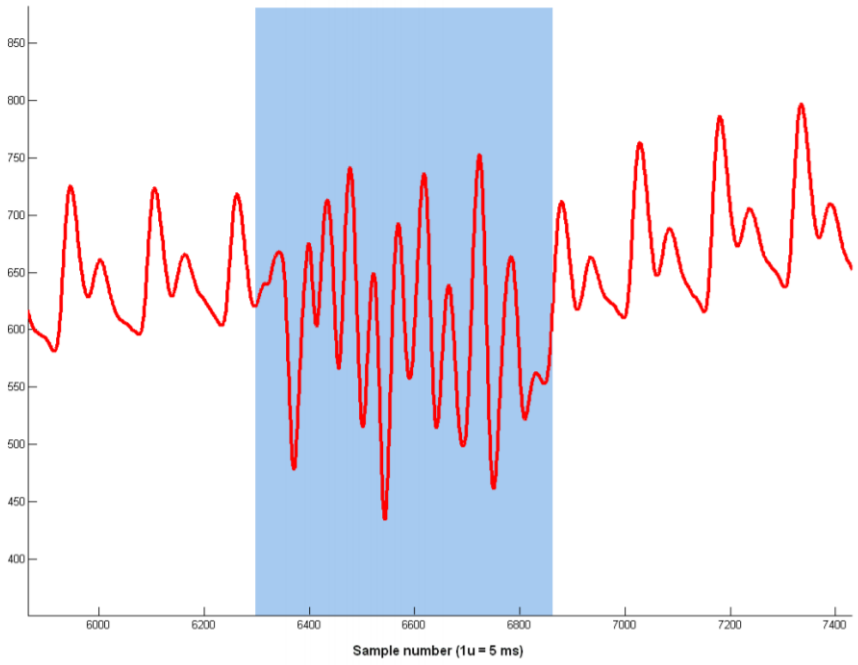

Figure 2.3: Example of the effects of motion artifacts in a PPG signal

had changed volume. Figure 2.3 shows an excerpt of a PPG signal and indicates the corruption by motion artifacts. In this example, it is clear that the motion artifact effects on the signal can have the same amplitude (and sometimes more) than the heart signal, making the heart rate extraction difficult and sometimes impossible.

On the other hand, the source of noise on ECG technology is caused by electrical muscle signals and bad contact with the electrodes. The muscle signals can corrupt the signal when movement is involved and also during respiration as the muscles of the upper thorax move. Additionally, movement can cause bad contact between the electrodes and the skin which translates into signal corruption. These events can happen during ambulance rides or during stressful conditions in the operation room.

2.3. State of the Art

2.3.1. Electrical Methods

Electrocardiography (ECG)

The first Electrocardiography measurement was performed in 1895 by Dutch doctor Willem Einthoven and it has become the golden standard for cardiovascular analysis. The electrical signals to stimulate the heart are conducted through the whole body and they can be measured in the skin. Electric potential difference is measured and it gives precise cardiac information about the depolarization and repolarization stages [2]. An example of the waveform profile is shown in Figure 2.4. A conventional 12-lead ECG is usually implemented to give a full analysis of the electrical conduction of the heart that include the diagnosis of arrhythmias, heart attacks, tachycardia, heart blocks, ischemia and other pathologies [20]. Simplified versions of the technology were developed in the late 80's and they became available for sports science measurements.

The leading provider in consumer grade ECG technology is the finish company Polar Electro with their signature chest band and smart watches. Other manufactures also have similar products with comparable concepts. Different approaches are being considered for drivers and other scenarios. ECG measurements are very precise if the electrodes are correctly positioned. The technology is considered so robust that it is commonly used as a control measurement to test new developed technologies [21].

One downside of the ECG is that the quality of the signal is related to the position of the electrodes. Additionally, it is sensitive to motion artifacts that can corrupt the signal [59]. In chest bands, the electrodes are near the heart which provides a stronger signal. For consumer applications, the chest band is a reliable device for HR measurement but it lacks in user comfort as it's an additional device that needs to be wet to work properly [23].

To solve these issues, two developments for upper body ECG were developed around the ear. The first research idea implements one lead in the ear and one the in the left arm. The team found that the ear lead is correlated to the ECG Lead I. The position of the electrodes also allowed for long term monitoring of the HR in stationary conditions [49]. Another development implement an electrode in the mastoid area and the second in the lower part of the neck. Both electrodes used were taped to the skin of the user and the signal was simultaneously measured with PPG and BCG signals. The results obtained were satisfactory but the tests were performed in stationary conditions also [26].

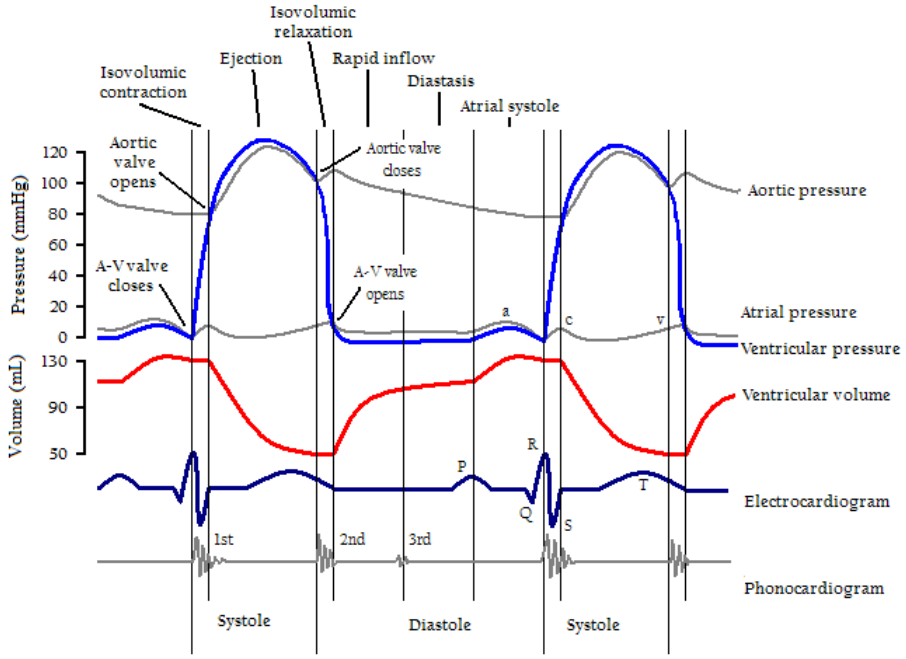

Figure 2.4: Cardiac events and resulting ECG and PCG signals

Impedance Cardiography (ICG)

Based on Ohms law, body tissue can be modeled as an impedance. Applying a current and measuring the resulting voltage in the tissue, the impedance is calculated. Changes in

impedance are caused by volume flows and can be used to characterize the cardiac system and respiratory systems of a patient. One typical distribution in medical devices positions the electrodes in the neck and the lower end of the ribs [50].

The measurement of the body impedance is a low-power and low-cost solution that does not require to be across the heart as the ECG. The main drawback of the technology is that it is very sensitive to motion artifacts and requires constant electrode contact [46].

Common measurement areas also include the feet, the wrists and the hands. To decrease the effect of the motion artifacts in the signal, different signal processing methods have been implemented. Fast Fourier transformation of the signal can be used to filter unwanted frequencies associated with noise. Multiple signal classification assumes the HR signal is uncorrelated to the noise signal and uses orthogonality to estimate the dominant frequencies [31]. No implementations are recorded to be located only in the head and tested high movements.

2.3.2. Mechanical Methods

Ballistocardiography (BCG)
When the heart pumps blood, the pressure in the blood vessels of the body increases. The volume of blood that flows through the aorta causes detectable body movements. These can be detected in different parts of the body and the periodic movement can be detected using different techniques. The most common ones are the visual detection of movement in a specific body part and acceleration measurements [63].

The visual detection is commonly implemented using cameras and has been applied for different applications such as stress monitoring. Using already implemented webcams in personal computers, an employer can monitor the HR of workers and estimate stress levels. It is an unobtrusive and non-contact solution but it is very dependent on the stationary position of the user. The technique tracks a specific position in the ear and records its micro-displacements to determine the HR using spectral analysis [13].

To measure the acceleration changes of the body, different surfaces have been modified such as chairs and beds, and more recently have been implemented in wearable devices [35]. The method use acceleration sensors to determine the ballistographic movements of the body [29]. This technique is especially suitable for situations where there is little to no movement and that require long measurements as in monitoring sleeping patients. Because the technique is based in measuring small-scale movements of the body, it is very sensitive by motion artifacts [64].

Phonocardiography (PCG)
Heart sounds are usually analyzed using a stethoscope. The heart sounds give information regarding the turbulence caused by the blood when leaving the atrio-ventricular valves and the semilunar valves as is shown in Figure 2.4. The correlation of the sounds with the systole and diastole start points can be used to calculate the heart rate. Using a microphone,

modern developments record the heart activity [55] .

This minimally invasive method is also useful when it is not possible to use other methods, such as measuring the heart rate in premature infants [4]. The technique is very sensitive to other sounds and movements [40]. Due to the noise levels required, no application was found that used PCG in sports science [54].

Pressure

The change in blood pressure changes the radius of the blood vessels with each cardiac pulse. This moves the surrounding tissue in the same frequency of the HR. The detection of these vibrations in the skin close to major arteries is what paramedics do to check if there is a pulse using their finger. Using this same principle, pressure sensors in direct contact with the skin are also able to detect the vibrations and to derive the HR if there is a main artery close [12].

Measuring positions are usually located in the wrists, chest and ears. The area needs to have a main artery that is surrounded by soft tissue. The measurements can be done using different technologies that have already been tested. Current teams have developed an array of MEMS capacitive sensors designed specifically for the changes in pressure of 10 to 100 kPa in which the tissue changes can be recorded [14].

Pressure changes can also be measured using piezoelectric sensors. Polyvinylidene fluoride (PVDF) is becoming very popular nowadays. This material is a fluorinated thermoplastic resin that has excellent chemical resistance [51]. The main advantage of this type of material is that it is flexible and easy to mass produce [52].

The availability and positive properties of the piezoelectric materials allow a straightforward implementation with the skin [53]. Wrist located sensors and in-ear located sensors have had considerable success in measuring the heart rate [39]. Unfortunately, the method requires constant contact and it is significantly affected by the motion artifacts [44].

2.3.3. Thermal Methods

While the human body can maintain a stable temperature throughout the whole body, a small difference between the core temperature and the one present in the outer parts of it arises caused by heat dissipation. Since the blood is pumped from the core of the body towards the extremities, there is a difference between the temperature in the blood vessel and the surrounding tissue caused by the process called bioheat transfer [6][16]. Each heart beat then changes the skin temperature at the surface that can be detected using a sensor with sufficient resolution. The measurement can be made with direct contact with the skin and in an unobtrusive way using non-contact technology.

Contact

Using high resolution temperature measurement in the wrist, temperature changes of 0.002 K were recorded using thermopiles. With a differential approach, this resolution could detect the change in skin temperature based on the blood flow [18][17]. The contact requirement introduces noise artifacts in case of user movement and reduces the comfort of the solution.

Non-contact

Based on the Stefan Boltzmann law on black body radiation theory, the human body radiates with a peak wavelength of $10\mu m$. Many commercial applications use this concept to calculate the body temperature in ear [47]. When the resolution of the device is maximized, the same working principle of the contact solution can be applied using a Far Infrared sensor. With a resolution of 0.02K, the changes in radiation show the change of temperature caused by the blood flow can be detected in the inside of the nose. Thermopile based infrared (IR) sensors can easily reach this resolution [8]. Similar approaches were implemented using IR thermal cameras with better results but with a minimal distance requirement [56][67][27][24].

2.3.4. Radiant Methods

Photoplethysmography (PPG)

Photoplethysmography is the most popular technology to monitor heart rate in a non-invasive way. This method uses light to detect changes in blood vessel volume. With each heartbeat, all blood vessels in the body expand and contract following the change pressure. PPG systems use a light emitter and a light detector [20]. The red blood cells have a characteristic absorption wavelength and so, the light can be absorbed or reflected based on this principle. Assuming the sensor is in a fixed position, then the difference in light detected is relative to the change in the quantity of the blood cells and consequently of blood volume. The systems can work in two ways, by light reflection and light transfer. In the first one, the emitter and detector are located side by side (smartwatches) while in the second one, the emitter and detector are located on opposing sides of the tissue (finger probes such as the one in Figure 2.5) [57].

Locations

PPG implementations were first located in the finger tips and the ear lobes in clinical applications [33]. These two locations are widespread in heart rate measurement and peripheral capillary oxygen saturation (SpO2) and experimental measurements have use also forehead measurements to take this measurement. Commercial implementations started appearing in arm bands and wrist bands for heart rate measurement. Ultimately, in ear measurement started also appearing in the market in the past few years [57].

Wavelength

In the first PPG approaches, Infrared wavelengths (around 880 nm) were preferred for

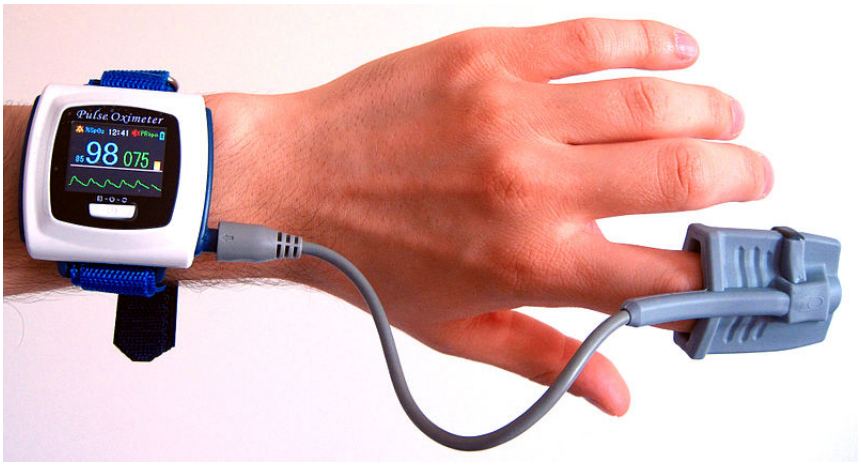

Figure 2.5: Example of a finger-based pulse oximeter

the fingertip and ear lobe measurements. These positions were used because they have very superficial blood irrigation [36]. The downside is that they are not comfortable for commercial applications. It was discovered that green light (around 525 nm) has better response and tissue penetration in other locations. This wavelength then became the most common emitter used [25] [37].

Signal Analysis

The main issue with PPG are the motion artifacts. Movements of the sensor in relation to the skin can cause signal disturbances in the same order of magnitude than the received heart rate signal. To try to reduce the effect of the motion artifacts (MA), different approaches have been implemented. Starting with simple moving average filters through Kalman filters, independent component analysis, principal component analysis and others [57].

Asynchronous filter

One approach that implements other theory is the asynchronous noise filtering. Redundant PPG measurements are taken in the right and left ear and it is assumed that the heart pulses are synchronous while the movement of the ear tips are not. By analyzing both signals, it is possible to filter the motion artifacts from the signal [60].

Adaptive filters

To try to quantify the movement of the sensor, acceleration sensors are implemented along with them. The quantification of the movement can give the information about the type of movement the sensor has and the magnitude of the expected motion artifacts [1][3].

The reliability of PPG signals been tested many times and the motion artifacts are still present in sports settings. The signal quality is unreliable when performing activities with high levels of movement [61][45][58].

Color
Another non-contact technique that is being developed is the detection by color variations. The change in blood volume during the diastole and systole periods changes the quantity of red blood cells and therefore the color of the skin. The difference in color of the face is commonly used to detect the HR. This technique requires standing still and works better for subjects with light-colored skin [19][10]. The technique is currently being studied in work environments and places with high flux of people such as airports. Color measurement is done in different frequencies including the infrared. The variation of skin color in the same person makes the technique extremely sensitive to motion artifacts [9][66].

Distance
The vibrations of the skin caused by the heart pulses can be detected using radar technologies. The research in this area focuses specially in the chest and neck of the user to detect the vibrations caused by the beats. The technology requires a minimum distance to detect the superficial changes. It is commonly used to monitor sleeping patients and for elderly care [62][22]. Since skin movement is translated to heart rate, motion artifacts represent the biggest noise source of the technique [15]. The minimum distance requirement also makes the technique not ideal for miniaturization [65].

2.4. Comparison and Selection

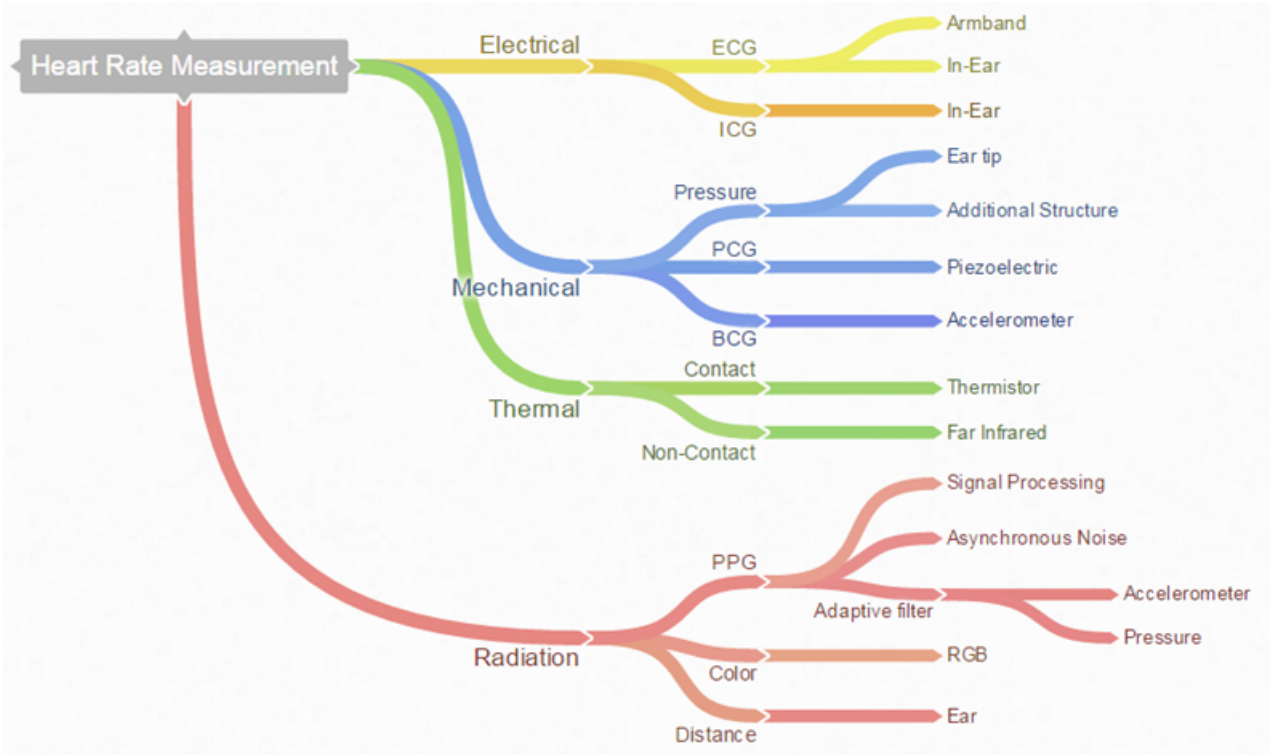

Figure 2.6: Summary of all heart rate detection methods covered

After all the information gathered a comparison was made between methods. A complete list of the methods of each signal domain is presented in Figure 2.6. With this informa-

tion, a rank system was proposed to evaluate each of the methods based on the previously stated requirements of the project:

- User comfort: How is the user experience affected.
- Quality of the signal: How clean is the signal measured.
- Motion artifact suppression: How much is the motion noise effect.
- Design modification: How is the current earphone design needs to be changed.
- Power consumption: How much extra energy does it require.
- State of the Art: How mature is the technology required.

For all the studied domains, every method that was feasible to implement in an earphone was given a rating from 1 to 6 (6 being the best) based on the literature found. Some methodologies had multiple options such pressure or ECG sensing. Since PPG technology is the most widely used and developed, more subdivisions were compared. A complete table was created and can be seen color coded in Figure 2.7.

			User Comfort	Quality of Signal	Motion Artifact Suppression	Design Modification	Power Consumption	State of the Art
Electrical	ECG	Armband	●●●	●●●●	●●●●●	●	●●●●●	●●●●●
		In-Ear	●	●●●●●	●●●●●	●	●●●●●	●●●
	ICG	In-Ear	●●●●	●●●●	●●●	●●●	●●●●●	●●●●●
Mechanical	Pressure	Ear tip	●●●●	●●●●	●	●●●	●●●●	●●●●●●
		Additional Structure	●●●	●●●●●	●	●●	●●●●	●●●●●●
	PCG	Piezoelectric	●●●●●	●●●●	●●	●●●●●	●●●●	●●●●●
	BCG	Accelerometer	●●●●●●	●●●	●	●●●●●●	●●●●●●	●●●●
Thermal	Contact	Thermometry	●●●	●●●●	●●●●	●●●	●●●●	●●●●●●
	Non-contact	IR Thermometry	●●●●●●	●●●●	●●●●●	●●●●●	●●●●	●●●●●
Radiation	PPG	Signal Processing	●●●●●	●●●●●	●●●	●●●●●	●●●●●	●●●●●●
		Asynchronous noise	●●●●●	●●●●●	●●●●●	●●●●●	●●●	●●
		AF: Acceleration	●●●●●	●●●●●●	●●●●●	●●●●●	●●●●●	●●●●●
		AF: Pressure	●●●●	●●●●●●	●●●●●●	●●●●	●●●●	●
	Colour	RGB	●●●●●●	●●●●●	●●●	●●●●●	●●●●●	●●●
	Distance	Radar	●●●●●●	●●●●	●	●●	●●●●●	●●●●●

Figure 2.7: Comparison of all the HR measurement methods

While PPG has the best performance in most of the requirements, it is also interesting how other technologies could attain similar results while being less sensitive to motion artifacts. The Non-contact infrared thermometry is a technique that has not been studied in depth, with smaller sensors, instead of advanced IR Cameras. Confirmed by the table, this technology was selected and approve by all the interested parties in the project for further analysis and implementation.

2.5. Bioheat Transfer

Once the technology was selected, it became important to understand thoroughly the concept of bioheat transfer that governs the method. Heat transfer is the exchange of thermal energy through different systems. While mechanical engineering usually studies homogenous materials, bioheat transfer studies the exchange in heterogenous biological systems. The theory of bioheat transfer is commonly considered to treat cancer tumors using ablation surgeries and heat dissipation of implantable devices.

Ablation surgery is a type of procedure in which tissue is destroyed. It can be performed by LASER, radio frequency or ultrasound. The tissue (Usually a tumor) is heated to denaturalize the proteins of the cells and kill them. In these procedures, it is key to understand how heat flows out of the tissue to know the exact amount of heat that needs to be inserted without affecting important surrounding tissue.

There are two different types of body temperatures that are used, core temperature and skin temperature. Core temperature is extremely constant and only varies 0.6 K except when there is an illness present such as fever. This temperature can change during exercise around 1 k and in extreme cold conditions it can decrease up to 2 K. Still, this changes

require a large amount of time in order to take effect. In contrast, the skin temperature changes from location to location and it depends on the temperature of the environment and other conditions such as wind and humidity.

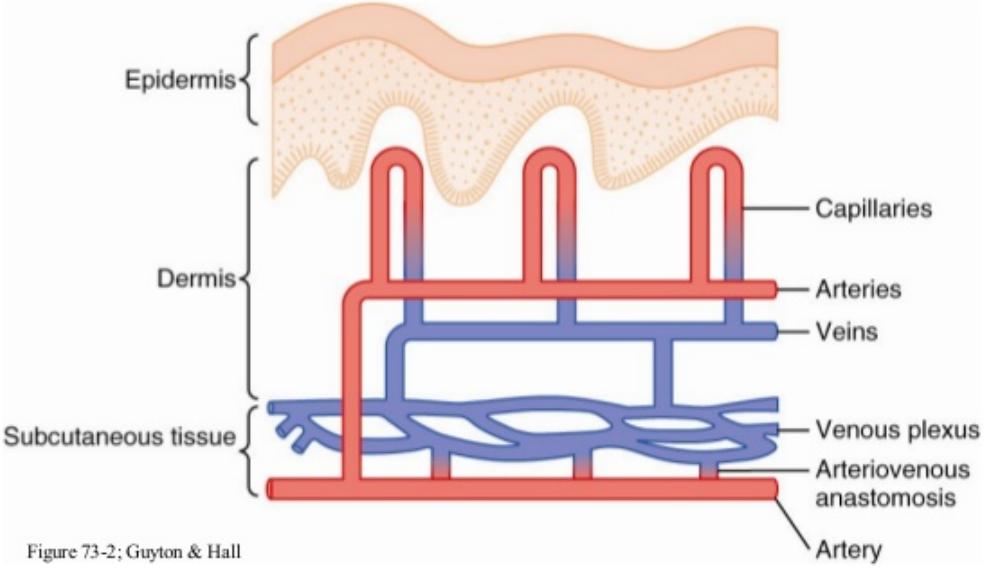

Figure 2.8: Tissue layers that separate the blood flow from the environment

The body's core temperature is developed in the central part of the body where the major organs are located (heart, lungs, pancreas, etc.) and it is transported by the blood through the arteries to the rest of the body. Because the environment is usually lower than the core temperature (37 C), there is a cooling effect from the skin to the environment and heat transfer from the blood into the surrounding tissue and to the environment takes place. This heat transfer results in changes in temperature that can be measured by infrared thermometry. The ear anatomy and its temperature distribution are therefore of key importance for placement of the sensor.

It is important to note that the blood flow into the skin venous system greatly depends on the control systems of the body, it can vary from 0 to as much as 30% of the total amount of the blood pumped by the heart. The name of this process is vasodilatation and it is controlled by the sympathetic centers located in the posterior hypothalamus. Vasodilatation can cause an increase of the heat transfer to the skin as great as 8 times and it can then improve the signal strength of the heat dissipation profile.

The skin is composed of many different types of tissues with different thermal constants. The first layer is called the epidermis and contains 5 different types of cell tissue. The second layer, called the dermis, is composed of irregular connective tissue and includes the blood vessels necessary to provide support for the epidermis and dermis systems. The heat then needs to transfer from the blood vessels through the dermis into the epidermis to be able to radiate into the environment. Also, the temperature loss from previous dissipations has also to be taken into account specially in the first bifurcations of the external carotid artery. While the mathematical modeling of the heat system of the ear is outside the scope

of the project, the tissue composition was still taken into consideration during the search for strong heart beat signal.

2.6. Ear Anatomy

2.6.1. Tissue composition

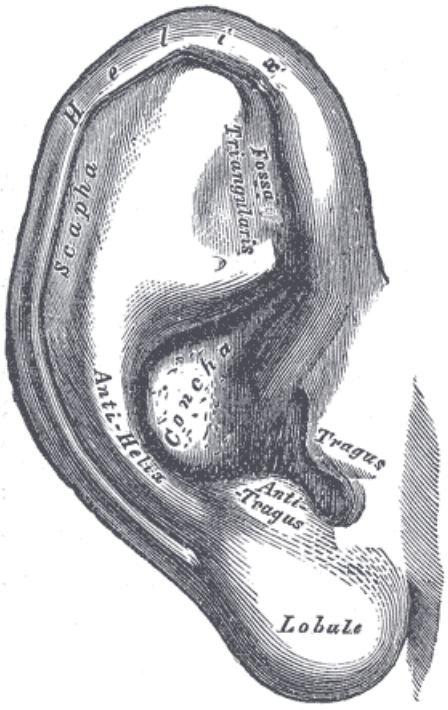

Figure 2.9: Names of the auricle parts

The ear is composed of 3 main parts, the outer ear, the middle ear and the inner ear. In non-invasive techniques, only the outer ear is considered. The outer ear contains the auricle (shown in Figure 2.9), the ear canal and the external layer of the tympanic membrane [41]. The tissues present have different irrigation levels, mechanical properties and thermal properties. The auricle is composed of yellow elastic cartage while the ear canal has more fat tissue in its composition [48]. The majority of HR earphones focus the light to the region between the anti-tragus and concha of the ear. According the HR sensor manufacturer Valencell, this part "comprises a bank of arterioles that expands like a balloon every time the heart beats, which provides a nice pressure wave for optical biometric sensors to measure blood flow" [43].

2.6.2. Blood irrigation

The main blood vessels present the middle ear are the internal carotid artery and the internal jugular vein as shown in Figure 2.10. Most of the blood irrigation comes from the aortic artery. The more vascularized the tissue is, the better optical technologies are. Methods that use changes in volume benefit from a short distance from a main blood vessel and a low amount of tissue separating the surface and the vessel. A high amount of fat tissue di-

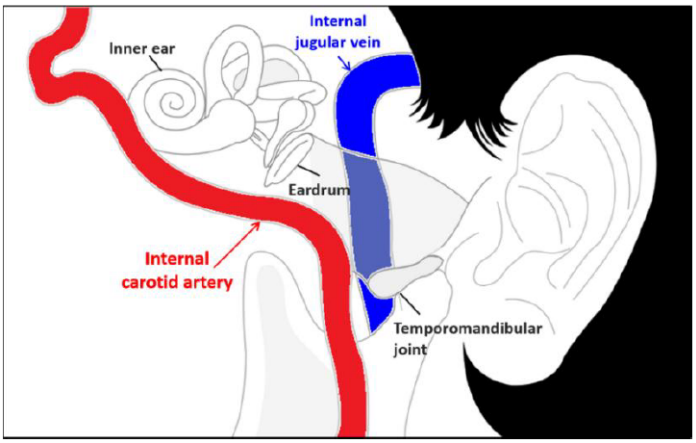

Figure 2.10: Blood vessels located near the inner ear [44]

minishes the signal that can be detected.

For the external ear, the main arterial vessels are the posterior auricular artery (PAA) and the superficial temporal artery (STA). The PAA starts irrigation in the back side of the auricle and then bifurcates to the central part of the external ear. Meanwhile, the STA starts in the posterior side of the ear canal and irrigates all the exterior locations around the ear auricle. The blood distribution locations of influence can be seen in figure 3.1.

2.7. The Wearable Issue

Current technologies can obtain adequate results in resting conditions but struggle under high movement activities. Most of the optical solutions, and specially the PPG solutions are known to have reduced accuracy with high amount of movement. The ECG bands by polar are design to not suffer this effect but they lack user comfort. Additional, there has not been relevant research on the effect of non-healthy subjects with this kind of measurements. A high concentration of body fat could reduce significantly the signal quality. Accumulation of fat in the wrist is more common than in the ear tissues [7].

To have constant monitoring, the user comfort is crucial. To have a good signal quality, the optical solutions currently in the market usually require a good fit. This translate into a tight grip in the wrist that can be uncomfortable for the user in the long term or an unreliable signal. The battery life of a device can also be a decisive factor in usability [5]. According to a study published in 2014, one third of the users stop using the wearable device after six months. By the 18th month, only 50% remain [30]. On the other side, people are already using earphones during exercise constantly [11]. The next generation of wireless devices (pushed by the iPhone drop of 3.5mm connector) makes Bluetooth earphones even more interesting as locations for biomedical sensors.

2.8. Requirements

The main constraints in the project are sensor size and sensor accuracy. The limited space available in a wireless headphone is also an important challenge since every inch available

must be shared with audio processing and battery systems. Other important requirement is a low power consumption. Battery life is one of the key aspects in wireless earphones and a sensor that consumes too much power will ultimately affect the device life time and usability. Finally, the comfort of the user is also a key factor. If the sensor requires a tight fit with the skin, it might cause pain to the users over prolonged use periods. The solutions that are to be devised need to modify the least amount the comfort that the original design of the headphones has. In the next section, the design considerations of the system are explained based on the information presented and this requirements.

3

System Design

3.1. Ear Location

The ear is a location where other electronic devices, such as the earphones of a headset and hearing aids, are already placed or can be placed with minimum discomfort during exercise. Also, it has the advantage of reduced movement compared to most other parts of the body. Based on the review of the anatomical distribution, 2 locations were selected based on the proximity to the PAA and STA arteries and contact with the earpiece. The blood flow through the superficial temporal artery was located in the antitragus while the blood flow of the posterior auricular artery was located in the Cavum Conchae.

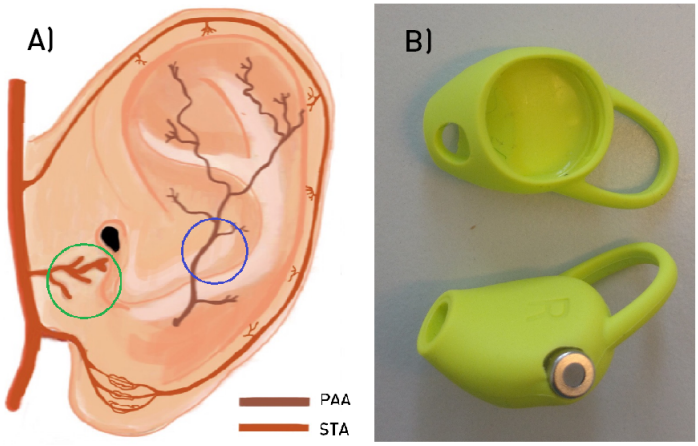

Figure 3.1: A) Distribution of arteries in the external ear. The green circle signals the anti-tragus and the blue circle signals the cavum conchae. B) Earpieces with corresponding modifications of the positioning of the sensors

The A section of figure 3.1 shows the location of the arteries in the external ear and the locations that were selected to be studied. In the B section, the earpieces show an example of the position of the sensor to study each of the locations. The upper earpiece positions the sensor towards the anti-tragus while the lower earpiece positions it towards the cavum conchae.

For the second part of the project, a central location around the cavum Conchae was selected. The size of the sensor limited the ability of the sensor to be arrange in different positions. Nevertheless, two locations were studied for the sensor. The first is the sensor in close range of the skin while the second location separates the sensor from the skin 1 cm.

3.2. Infrared Sensor

The selection of the sensor was based on 3 main items based on the bioheat transfer and blackbody radiation theory.

- Wavelength
- Size
- Responsivity

Wavelenght

The human body core temperature is usually located at 37 degrees Celsius. In this temperature, black body radiation emits at a frequency peak of $10\mu m$. The majority of the thermal radiation sensors are usually used to measure objects at very high temperature in which contact measurement is not convenient. Temperatures around 200 and 300 C emit at a wavelength between 1 and 5. The majority of the infrared detectors operate at these wavelengths and are not designed to measure human skin temperature.

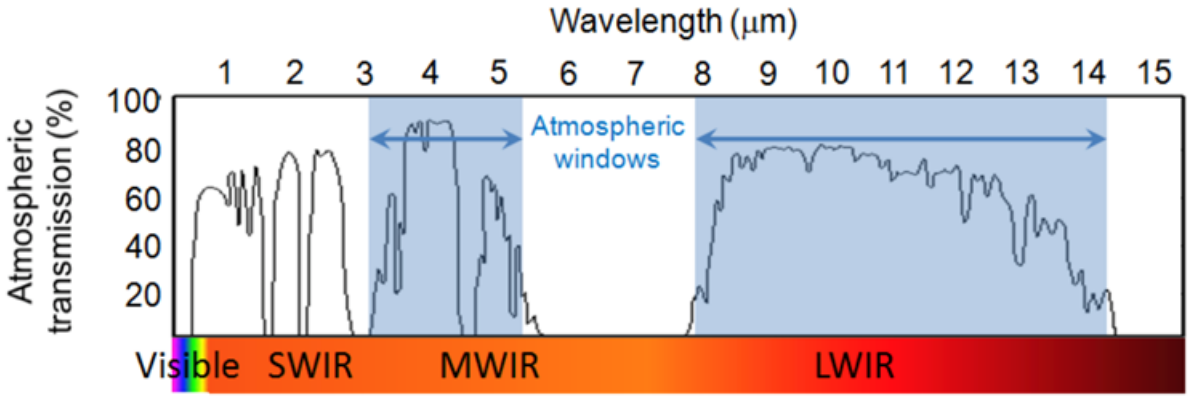

Figure 3.2: Atmospheric transmission of IR signals. The second atmospheric window contains the radiation of the human skin

The technologies that operate at this wavelength are pyroelectric detectors, bolometers and thermopiles. The pyroelectric detectors use crystal structures that are polarized and produce voltage when the temperature changes the structure of the atoms. While the pyroelectrics have the highest signal output, they also suffer from the micro-phonic effect in which small vibrations can also change atom structure and produce very high noise.

Bolometer arrays are usually implemented in commercial infrared cameras and the size of the available sensors is not suitable to be implemented in a prototype for an earpiece. The thermopile detectors are large amounts of thermocouples organized in parallel in order to increase sensitivity. Thermocouples have two different materials that produce a differential potential when subjected to a temperature change. These type of sensors are the best in terms of cost-efficiency and are widely available in the market. Because of all the positive aspects of this sensors, they were selected to be the best approach for this application. Furthermore, these type of sensors are usually implemented with a filter for the $8 to 14 \mu m$ wavelength that is conveniently centered around the $10 \mu m$ peak wavelength of the body temperature maximizing the received radiation. These wavelengths are usually refered to as Long waver Infrared (LWIR) and their localization in the spectrum can be seen in figure 3.2.

Size

Commercial developments of thermopiles are usually encapsulated in Transistor Outlines (TO) with the most common sizes being TO5 and TO46. The size of the sensor is very important to be able to position the sensor in different locations in the ear. The sensor size is also related to the active area size of the sensor which is the area that is sensitive to the infrared radiation. During the selection of the available sensors, a size of TO46 was preferred and studied but the TO5 was also used.

Figure 3.3 shows a size comparison of an earpiece, a 2 euro coin, a TO5 sensor (left) and a TO46 sensor (right). It is important to note that while the TO5 size can fit inside an earpiece, the mobility it has inside it is limited and could become a bigger issue if the speaker and electronics where to be placed back in. In contrast, the TO46 size can be moved more freely inside the earpice.

Responsivity

The responsivity of the sensor is the magnitude of the sensor output per unit of input. In case of a thermal detector, the responsivity corresponds to the voltage level per watt detected. While a high responsivity is favorable, the noise of the sensor also needs to be taken into account in order to understand the sensor performance. The noise is related to the resistance of the sensor in a relation to the fourth power of the temperature. The two relationship between noise and responsivity of the thermopiles is called Noise Equivalent Power (NEP).

With a list of all the thermopiles available in the market, the sensors were compared based on the NEP, size and availability. The selected thermopiles to be used were the TO5 Melexis MLX90615, the TO5 ST150 from Dexter Research and the TO46 ZTP-135SR from Amphenol. The Melexis sensor is a digital sensor with undisclosed performance values but boast a 20 mk resolution. The ST150 has a responsivity of 39.8 V/W and a NEP of 0.91 $nW/\sqrt{Hz}$. Similarly, the ZTP-135SR has a responsivity of 62 V/W and a NEP of 0.51 $nW/\sqrt{Hz}$.

Figure 3.3: Size comparison of an earpiece, a 2 Euro coin, a TO5 sensor and a TO46 sensor

3.3. Signal Processing

The heart rate value extraction from the raw data is a key aspect of the system. The output of the sensor requires several filter types and the shape of the waveform is not static in time. Several paper have been published about the extraction of heart rate in PPG signals and the use of different approaches ranging from filters to machine learning. The signal of the heart beats is not constant and it can change frequencies in 2 seconds. The standard frequency analyses are not able to detect this localized changes in frequencies.

In order to analyze the signals, one filter per signal was used. In the ECG signal, a low pass filter was implemented in order to filter out the R peak and leave only the more pronounce T peak. An example of the waveform can be found in Appendix A. This allowed for an easier calculation of the heart rate in the signal. For the infrared signal, a subtraction of the DC level was implemented using a low pass filter. The DC was calculated over 3 seconds of signal (300 data points) and it reduced the error caused by the respiration rate and slow temperature drift of the sensor and the measured skin area.

The continuous wavelet transform (CWT) is similar to the Fourier transform in that they both use inner products to quantify the similarity of a signal and a function. In the case of the Fourier analysis, the analyzing signal is a sine wave and it oscillates forever which makes the analysis not located in a specific time and frequency. In the case of the wavelet transform, the signal is a short wave that can change by scaling the waveform and shifting it through time. Different wavelets have different forms and choosing one from another depends on the wave profile that wants to be analyzed. The main property of wavelets is that they are not infinite like the sine waves but rapidly decaying signals. This makes the correlation of the analysis well localized in time and in frequency. An example of the code

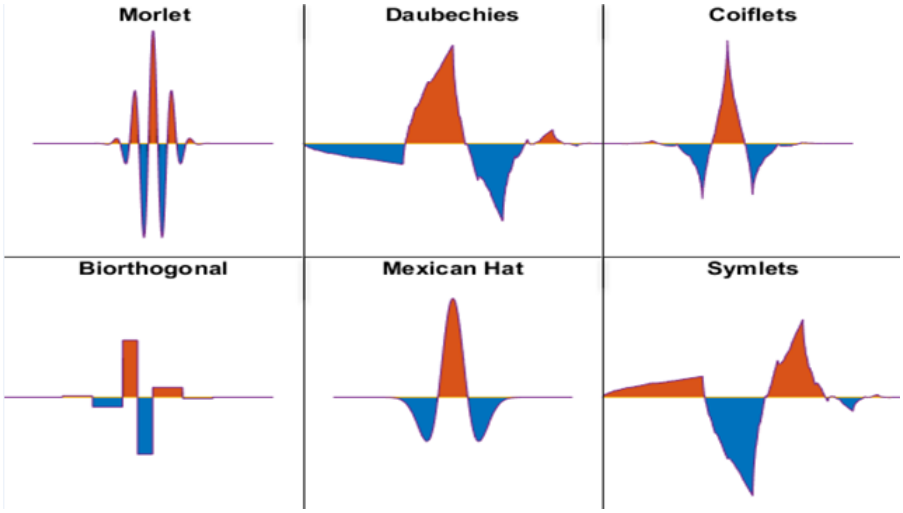

Figure 3.4: Different types of wavelets available for CWT

can be found in Appendix B and an example of wavelets commonly used can be seen in figure 3.4. In this project, different wavelets were implemented and the one that produced the best results was a variation of the mexican hat.

4

Experimental Designs

4.1. Digital sensor

Based on previous projects on infrared thermometry [8], a digital sensor with similar characteristics was chosen for the replication of the experiment. While the exact reference of the sensor used was not disclosed in the publication, the temperature resolution of the sensor was reported as 20 mK. The MLX90615 sensor has this exact temperature resolution and was so similar results ere expected.

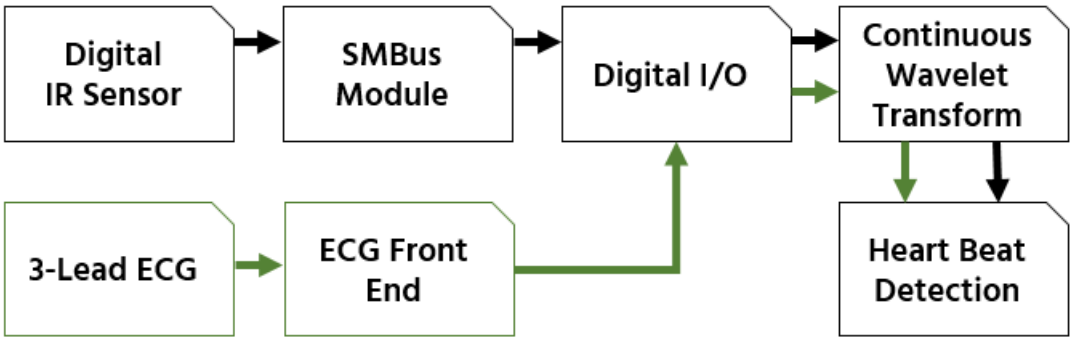

Figure 4.1: Block diagram of the system used to take measurements with the digital sensor

The digital sensor uses a System Management Bus (SMBus) protocol on a low voltage (2V). In order to connect it to a controller logic, an additional SMBus module was implemented. The output was read using the serial reader of an Arduino Uno board. An ECG module was also connected to the Arduino board to serve as a control. By having the exact location of heart beats, the comparison between signals can be more precise. More information about the ECG module used can be found in Appendix A. The system for infrared measurements using the digital sensor can be seen in figure 4.1.

Locations

As the first measurement being taken, the locations were chosen to provide information about the thermal information of the skin in different parts of the body. The nose was selected as a way to try to replicate the experiments of the previously published paper. The

wrist thermometry was studied using contact thermocouples and the neck was also selected as it had been studied using infrared cameras. Finally, the inside of the ear was selected as the final location to see if the signal is as detectable and comparable as the other locations.

4.2. Noise Equivalent Temperature Difference (NETD)

The NETD of a sensor is the minimum value of temperature that can be measured. It is the temperature in which the signal of the sensor is equal to the noise level. Temperature changes below this point will be masked by the noise signal. While some manufacturers do report the NETD of the sensors in the datasheet, the standard is to report the temperature while measuring a blackbody at 500K. The goal of this experiment was to study the NETD around the temperatures of the human body (303.15K-313.15K). In order to analyze the NETD of the sensor, a peltier cooler with a Pt100 reference sensor were used to measure temperature fluctuations.

The peltier cooler is a thermoelectric element that uses the peltier effect to transport heat from one side to the other. This effectively causes to heat one surface while cooling the opposite one. The peltier element was connected to a power transistor and a signal generator in order to cycle the power of the cooler using a square signal. The frequency and current of the system was modified in order to change the time that the element had to cool off and the magnitude of heat transported.

A Pt100 temperature sensor was placed in direct contact with the peltier element in order to measure the temperature changes. The thin film sensor changes resistance in response to this changes. The resistance change was measured using a high-resolution ohmmeter. In order to import the data with an exact timestamp, the ohm-meter was connected to a PC using a General Purpose Interface Bus (GPIB) interface cable. The data was imported using MATLAB.

The thermopile selected for this measurement was placed in front of the peltier cooler and the pt100 sensor and was fixed using an optics set up as shown in figure 4.2. The sensor output was measured using a nanovolt-meter and connected also to the GPIB interface. This set-up allowed to extract the temperature from the peltier element using the pt100 and the perceived temperature using the thermopile at the same time. The block diagram of the complete system is presented in figure 4.3

Using this set-up, 3 different tests were performed. The first changed only the current of the peltier element effectively changing the temperature of the surface from 299.15K to 314.15K. When the temperature stabilizes, measurements from the pt100 and the thermopile are collected to produce a sensor responsivity equation.

The second measurement powered off the current to the peltier cooler and let the temperature stabilize over a long period of time. When the voltage was taken from the thermopile, only the noise was visible. The standard deviation of the sensor output is used as the noise voltage level for room temperature. With the responsivity of the sensor and the

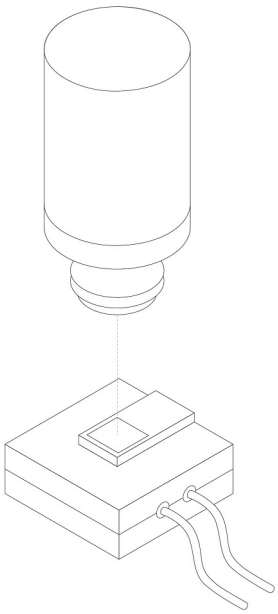

Figure 4.2: Diagram of the set-up of the thermopile, the Pt100 temperature sensor and the peltier cooler

noise voltage level, it is possible to calculate the NETD of the sensor.

The final test had a fixed current supply but variations on the frequency of the squared signal. The goal was to find if the NETD found using the responsibity and noise of the sensor was the same detected as the frequency of the signal grew.

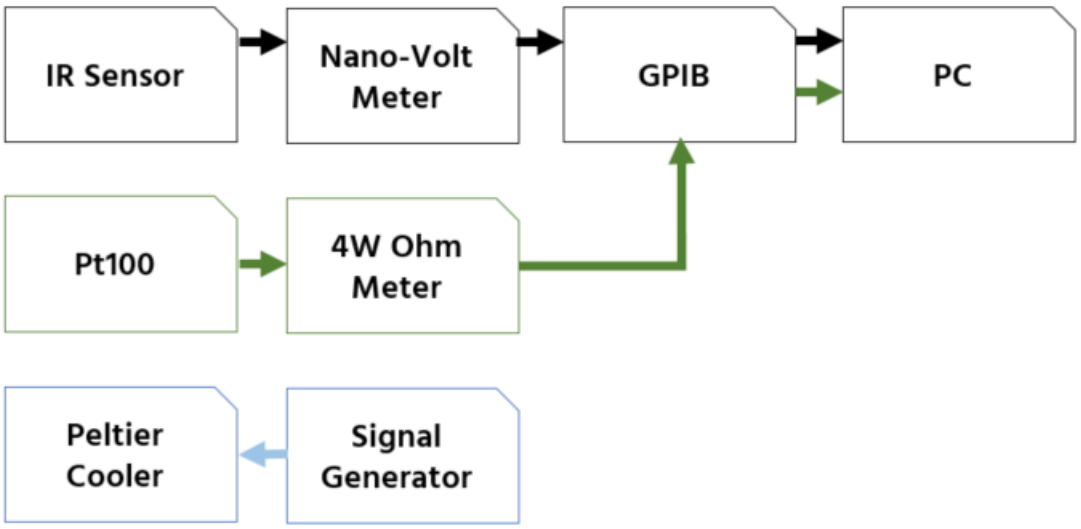

Figure 4.3: Block diagram of the system used to take measurements to find the NETD of the sensor at ambient temperature

4.3. Proof of concept test

While the nanovolt-meter had a very satisfactory resolution, the integration time of the signal was too great to be able to read the heart rate signal. Because of this, for the new measurements, the sensor output was read using an amplifier circuit. The amplifier was connected to an analog to digital converter (ADC) to be imported through MATLAB. The 3 lead ECG was also connected to the ADC to have time congruency between the signals. The measurement locations can be seen in figure 4.4 and the diagram of the system is presented in figure 4.5.

This new measurements aimed to discover if the analog thermopiles were better than the digital sensor, as they were not affected by a resolution cap and had better time constants. The goal was also to detect the heart rate in the neck, where other research groups had had success, and compare it to the signal of the ear. The locations that were studied were the cavum conchae, the neck and the wrist. Two subjects were studied and two repetitions per subject were taken. The test recorded 120 seconds of physiological data per sample.

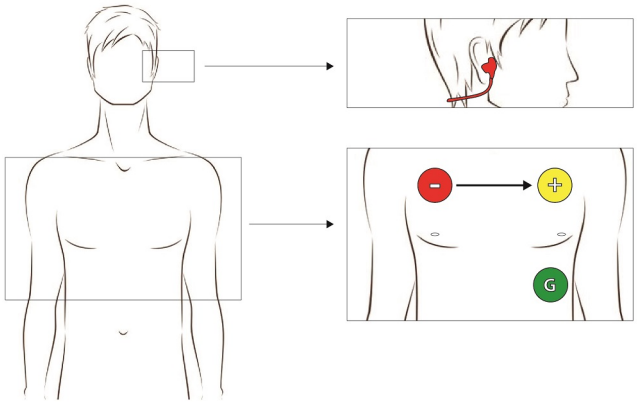

Figure 4.4: Location of the thermopile in the ear and electrodes used for the measurements of infrared thermometry and ECG

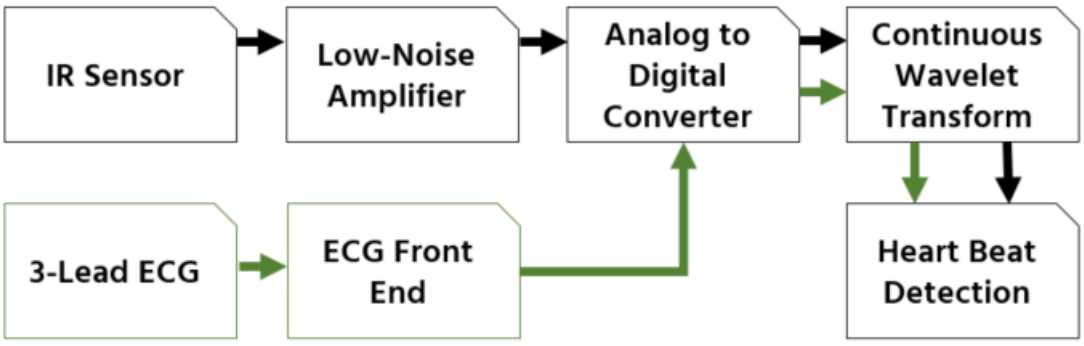

Figure 4.5: Block diagram of the system implemented to take the first measurements of the thermopile ST150

4.4. Arterial irrigation test

A test to study the performance of small sized TO46 sensors and the influence of the two main arteries of the ear was developed. The sensor was pointed at the cavum conchae (Location A) and the antitragus (Location B) in order to compare the two locations.

The amplifier board was used with the implemented low noise amplifier, low pass filter and proper shielding. More information about the modules used and the board can be found in Appendix A but a block diagram of the system is presented in figure 4.6. A fan was used to force cooling into the skin. 4 different type measurements were taken:

- Location A
- Location A with forced cooling
- Location B
- Location B with forced cooling

3 subjects were studied with 3 measurements per treatment. A total of 36 measurements were taken for the experiment. Each test consisted in 60 seconds of physiological data. The data was sampled at 100 Hz.

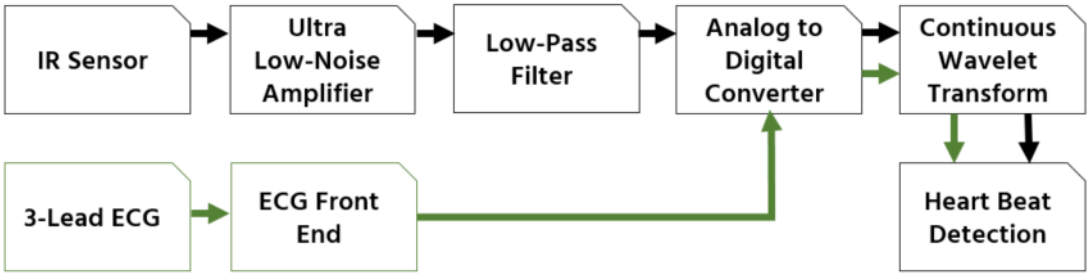

Figure 4.6: Block diagram of the system implemented to take the low noise measurements using the analog thermopiles

4.5. Area of measurement test

The last test set-up utilizes the same amplifier circuit as before and the same system as figure 4.6 but with the TO5 thermopile ST150 instead of the ZTP-135SR. The measurements were performed on the central part of the cavum conchae at 2 different distances, proximal to the skin and at a separation of 1 cm. The goal of the measurements was to find the effect it has to increase the effective area of measurement of the skin. For this measurement, 4 subjects were recorded for 5 sample of 60 seconds.

5

Results

5.1. Digital sensor

The digital sensor has a resolution of 20mK which is noticeable in the results. The output of the thermopile is limited digitally to ensure a good temperature measurement. Quantization error is the most important feature of the recorded output. The minimal step the sensor can output is very close to the noise level and the signal of the heartbeat. Because of this, the small variations of the heartbeat can be masked easily by the noise.

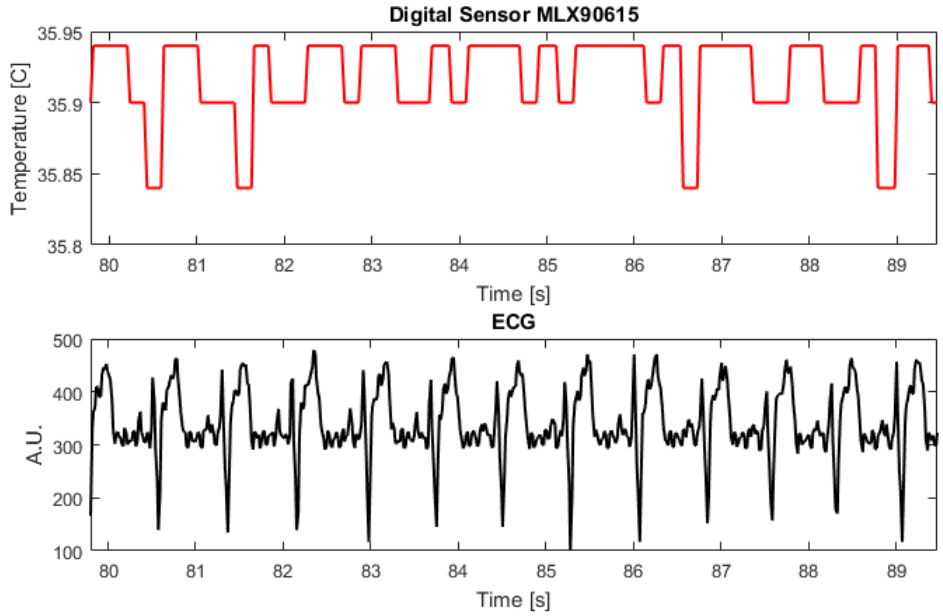

Figure 5.1: Excerpt of the output of the Digital sensor and corresponding ECG signal of a sample in the ear

Figure 5.1 shows an extract of the digital signal output from the ear. The lower part of the figure corresponds to the ECG signal from the heart of the subject at the corresponding time. It is clear the quantization error from the resolution of the sensor. While it is possible to match some of the peaks in the infrared signal to those of the ECG, some of the peaks also occur in the middle of the heart beat with the same amplitude (minimum step).

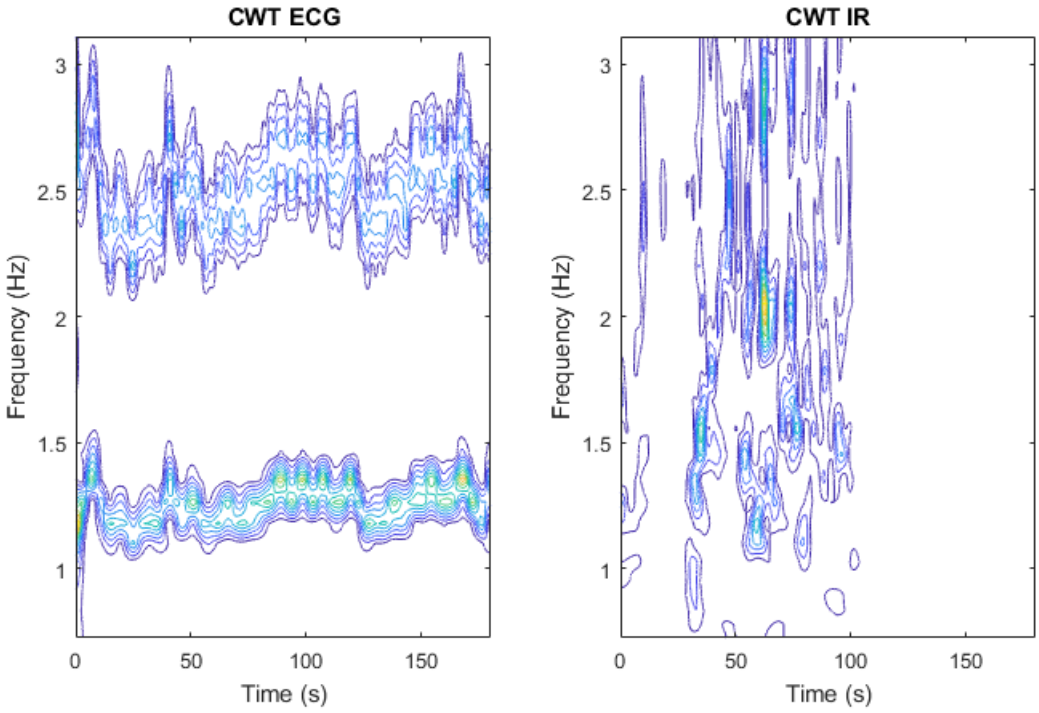

Figure 5.2: Contour plot of CWT coefficients of the ECG signal and the digital infrared signal from a sample in the ear

After the signal processing of the output, a continuous wavelet transform of the signal was performed and the results are shown in figure 5.2. The figure shows the CWT of the ECG signal on the left and the infrared signal on the right. The CWT graph shows the correlation coefficient between the signal and the wavelet. The brightness of the color shows how correlated are the wavelet frequency and the signal.

In the ECG signal, it is very clear to see the frequency of the signal fluctuates between 1 and 1.5 Hz corresponding between 60 and 90 BPM. It is also visible a harmonic of the signal at twice the frequency but with more spread of frequency and less magnitude of the signal. On the infrared signal it is not possible to detect a pattern that could correspond to the corresponding heart rate.

With the wavelet transform values, the maximum value of each second was calculated in order to find the frequency that has the strongest correlation with the wavelet. The results are shown in figure 5.3. While the ECG signal is fairly stable at around 75 BPM, the IR calculation is scattered over the whole range.

With the heart rate extracted using this method, the correlation between the HR extracted from the ECG and the HR extracted from the IR can be compared. Over the whole test, it was calculated how much the two heart rates are similar with a percentage of correlation. The percentage of similarity was calculated using 3 ranges, within 3.5 BPM, 10.5 BPM and 17.5 BPM.

Calculating this figure of merit every sample, allowed to quickly compare the results in a quantitative way. However, sometimes it is possible to have error due to the locking of the harmonic. Figure 5.4 shows the wavelet transform of a sample from the neck in which the harmonic is more clear than the general signal.

This behavior is not common and can be solved in the future with intelligent algorithms

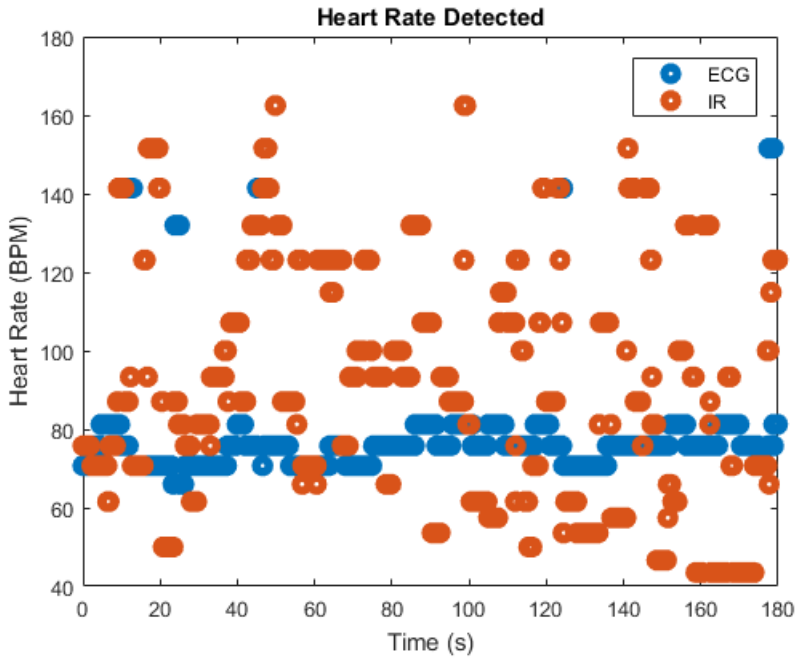

Figure 5.3: Heart rate detected from the digital sensor signal (Orange) and ECG signal (Blue) from a sample in the ear

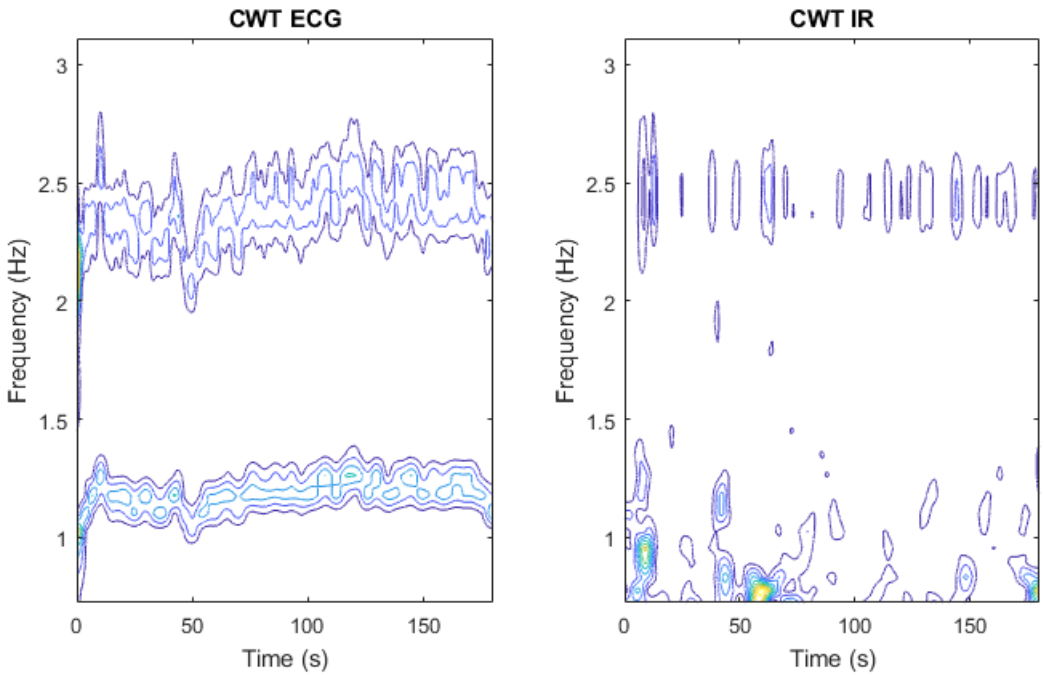

Figure 5.4: Contour plot of CWT coefficients of the ECG signal and the digital infrared signal from a sample in the neck

that understand that it is physiologically impossible to double the heart signal in 1 second. The complete table of the correlation percentage is shown in table 5.1.

Table 5.1: Correlation percentage results based on location of the digital sensor

Location	±3.5 BPM	±10.5 BPM	±17.5 BPM
Ear	3.6	13.1	20
	3.5	16.9	24
	6.2	17.3	31
Neck	1.0	5.6	16
	1.6	5.3	9
	5.1	13.0	18
Nose	1.9	6.0	7
	0.0	5.9	6
	1.3	10.7	21
Wrist	0.0	4.6	18
	3.7	10.7	11
	0.9	5.8	17

The results do not show a strong correlation between the heart rate calculation from the infrared and from the ECG. In the first range, the percentage does not surpass 10%. This is mainly due to the quantization error. Because the resolution was not modifiable, the digital sensor was discarded in favor of a sensor with analog output.

5.2. Noise Equivalent Temperature Difference

To analyze the performance of the analog sensors, 3 different tests to find the NETD where performed. The responsivity regression was performed using 1600 data points which are very accurate.

The values of the test for the responsivity and noise voltages are presented in table 5.2. The average of the values was used to calculate the NETD in equation 5.1.

$$NETD = \frac{std}{Responsivity} = \frac{2.191\mu V}{41.971\frac{\mu V}{K}} = 52.215mK \tag{5.1}$$

Table 5.2: Responsivity values and noise levels of the ST150

	Test	
Repetition	**Regression Slope (uV)**	**Noise std (uV)**
1	43.6501	2.76075
2	40.1432	2.04500
3	42.1202	1.76893

According to the NETD, the sensor can detect temperature changes up until 52mk. The third test of the set-up allowed to analyze the minimum detectable temperature in a practical way. Figure 5.6 shows the data distribution of the temperature at different frequencies.

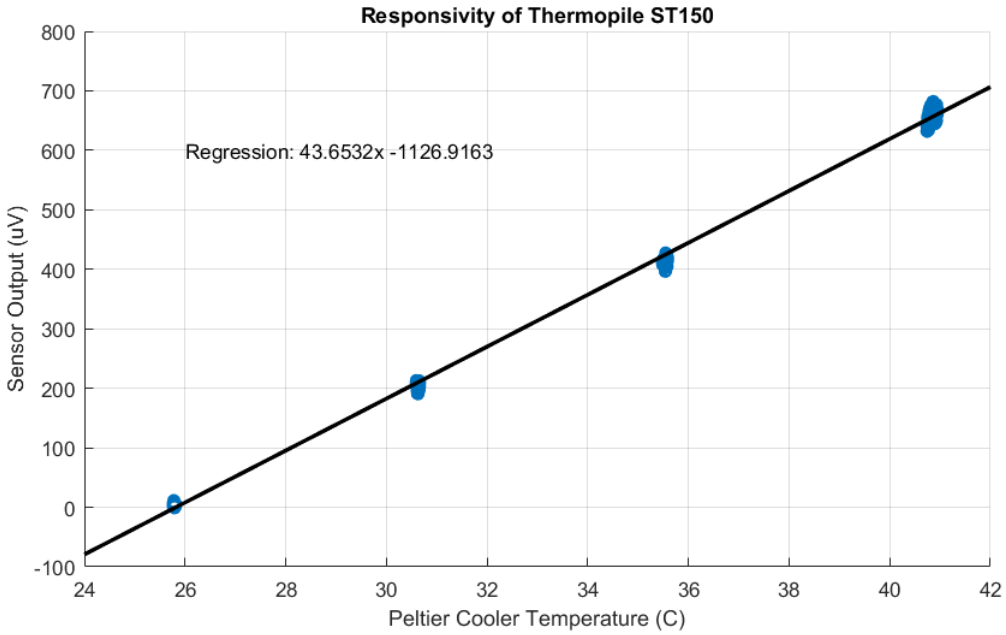

Figure 5.5: Linear regression of the Responsivity of the ST150 sensor

The temperature fluctuates between two points. The two sides become almost indistinguishable at 4 Hz when there is no longer 2 clusters at each side but rather a line connecting the two ends. The range of the x axis in the figure allows to confirm that the theoretical value of 52 mK is correct.

5.3. Proof of concept test

The first test using the low noise amplifiers aimed to proof that the system could detect the heart rate using the set-up. The analog output of the signal delivers a voltage output that corresponds to temperature. Because it was more interesting to detect temperature changes rather than the exact temperature of the tissue, a temperature calibration was not deemed necessary.

Figure 5.7 shows an extract of the ECG signal at the same time that the corresponding signal (after filtering) of the IR signal in the neck. This selected sample shows a fairly periodic signal that has a similarity with a sine wave. However, in the second part of the signal it is also visible the deterioration of the signal an how it can change waveform and become more difficult to detect.

Out of the all the locations, the neck was the one that was more promising from the literature review. Figure 5.8 shows the CWT of one of the neck samples. The ECG coefficients are very stable and bright with no presence of harmonics. The IR while not as bright as the ECG signal, it is stable in the same frequencies.

The heart rate estimation is then very clear and a very high correlation was calculated in this case. Figure 5.9 shows the calculated HR from both of the signals.

While the signals from the neck are the strongest ones due to the proximity to the carotid artery, the ear also produced relevant results. Figure 5.10 shows the CWT of an ear sample. While there is more noise present in the other frequencies, the correct heart rate can be calculated with good accuracy. Figure 5.11 shows the calculated heart rate from

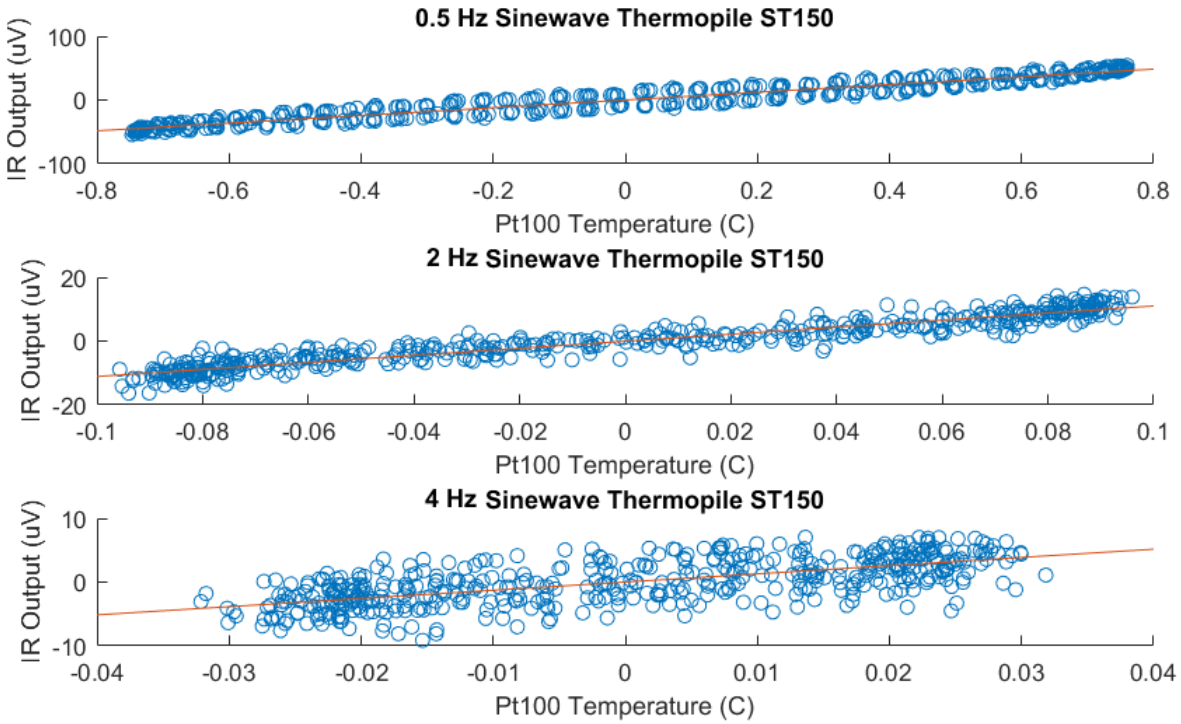

Figure 5.6: Behavior of the signal output of the ST150 at 0.5, 2 and 4 Hz

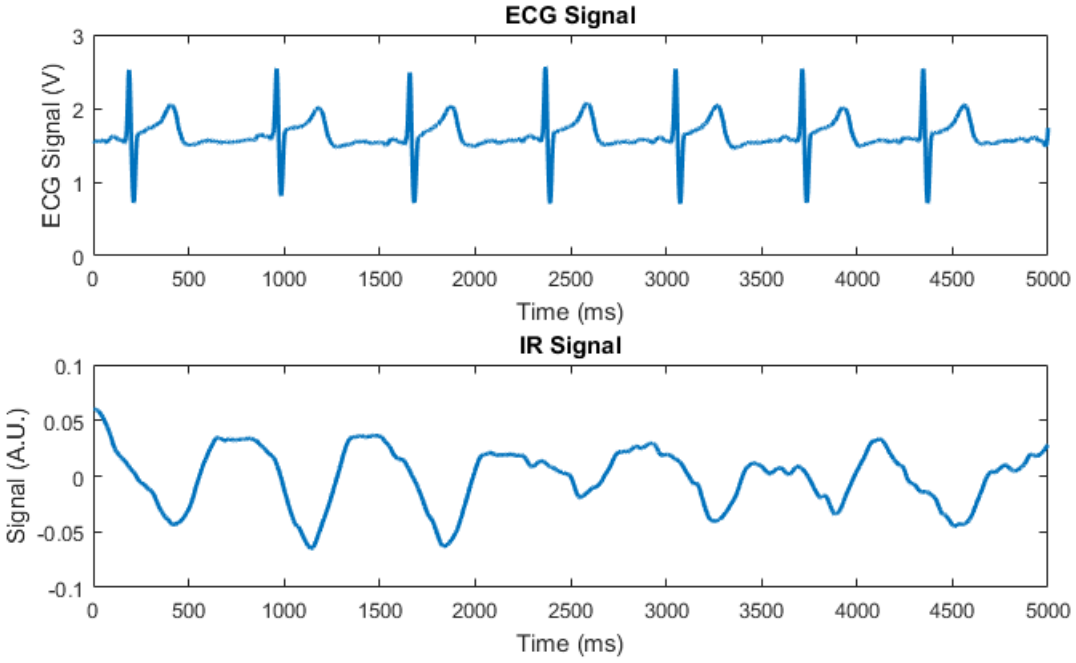

Figure 5.7: Excerpt of the output of the ST150 and corresponding ECG signal of a sample in the neck

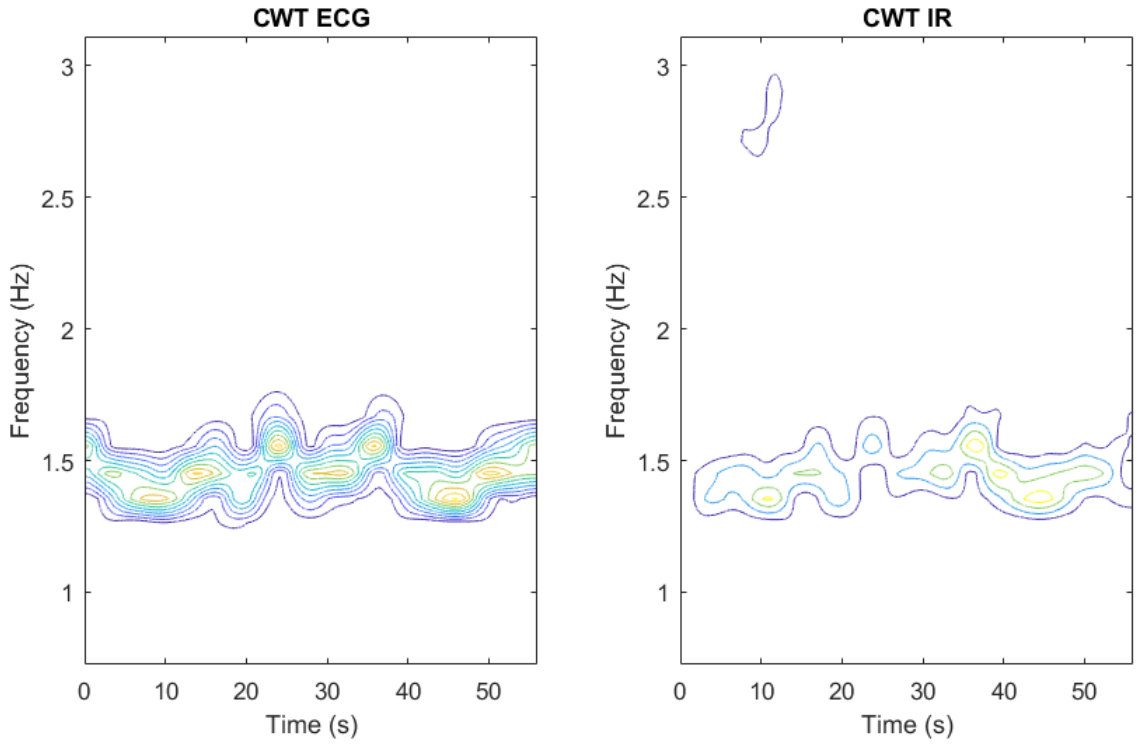

Figure 5.8: Contour plot of CWT coefficients of the ECG signal and the ST150 signal from a sample in the neck

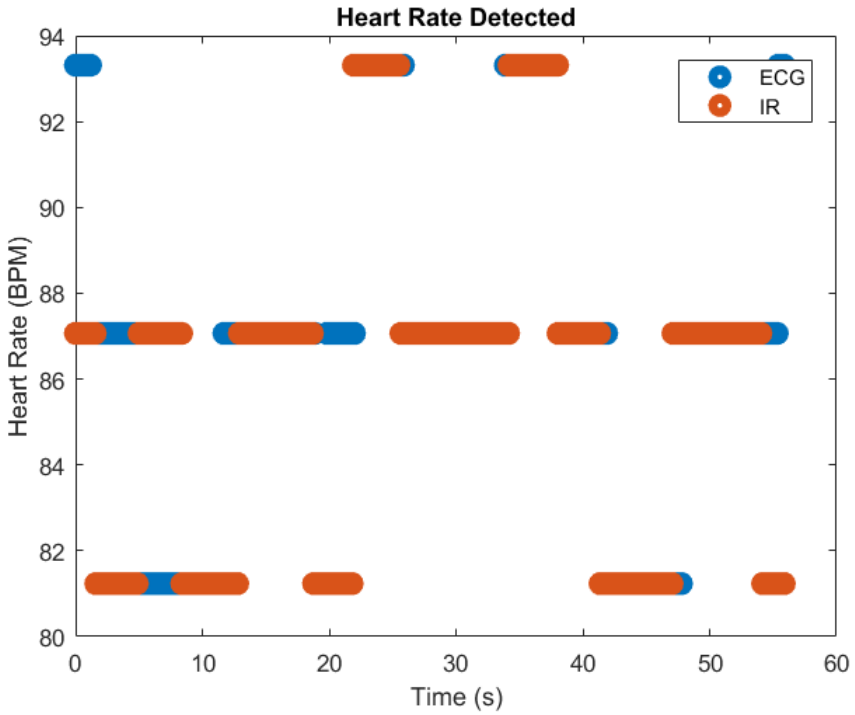

Figure 5.9: Heart rate detected from the ST150 sensor signal (Orange) and ECG signal (Blue) from a sample in the neck

the ECG signal and from the IR signal.

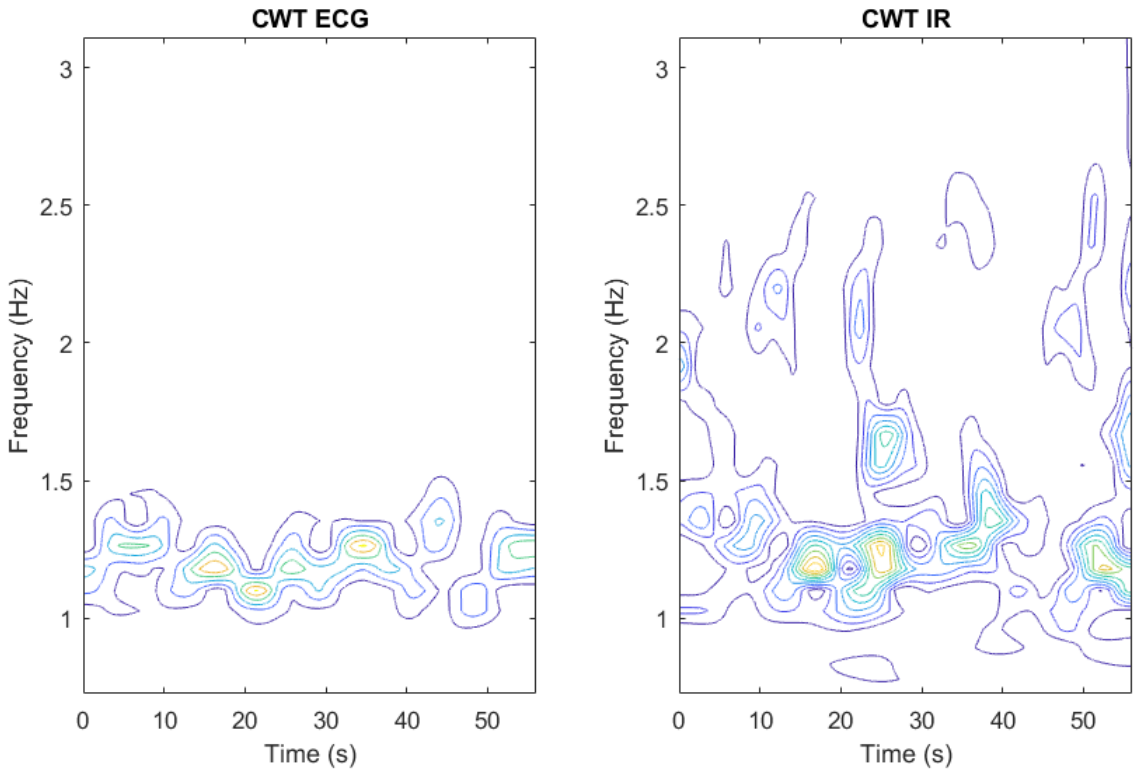

Figure 5.10: Contour plot of CWT coefficients of the ECG signal and the ST150 signal from a sample in the ear

The complete results for the correlation percentage is presented in table 5.3. The neck signal is the location in which the signal is stronger. The ear had the second best performance while the wrist had the worst. This results are shown in figure 5.12 as a boxplot. The red line corresponds to the median of the sample. The outer parts of the box corresponds to 50% of the samples and the limits correspond to the maximum and minimum values. Figure 5.12 shows the distribution of correlation percentages in the 3.5 BPM error range while figure 5.13 shows the distribution in the 10.5 BPM error range.

5.4. Arterial irrigation test

Two different treatments were investigated using the small sensor TO46, location and forced cooling effect. location A was selected as the cavum conchae and location B was the antitragus of the ear. The forced cooling was performed with a fan.

An improvement of the signal was expected by the fact that the small sensor had similar NETD than the ST150 thermopile and was located within better blood irrigated tissue. Unfortunately, while the NETD was similar, the active area of the sensor was reduced 4 times which reduced the total radiation that the sensor could detect. Additionally, the sensor was placed almost in contact with the skin. The sensor was only separated using an O-ring around the window to prevent contact. This made the detected area smaller than in previous measurements. The plan to find the arterial blood distribution was unsuccessful as none of the 36 measurements had significantly good results.

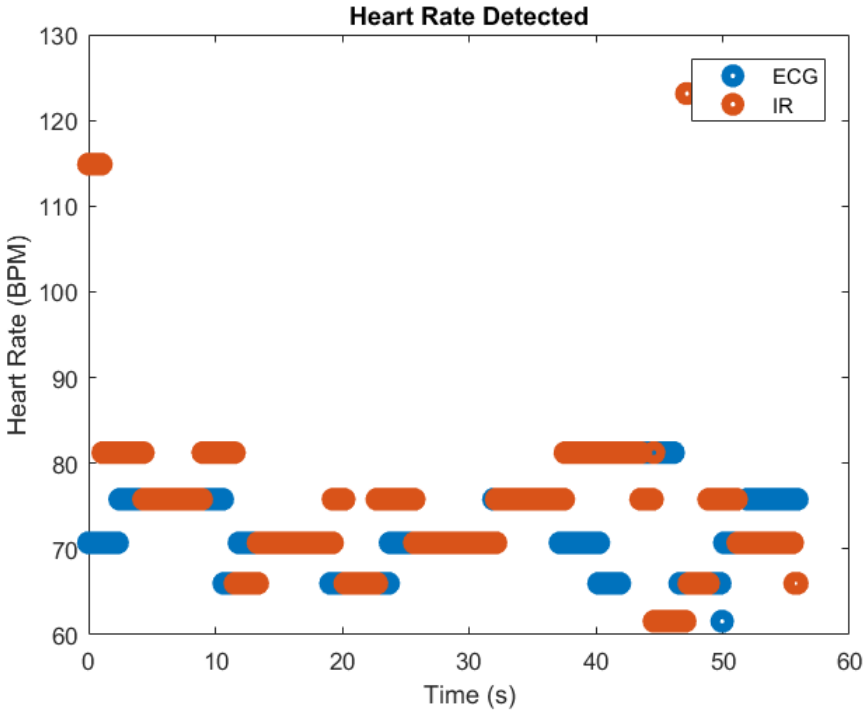

Figure 5.11: Heart rate detected from the ST150 signal (Orange) and ECG signal (Blue) from a sample in the ear

Table 5.3: Correlation percentage results based on location of the ST150 sensor

Location	±3.5 BPM	±10.5 BPM	±17.5 BPM
Ear	30.4	53	56
	45.8	68	78
	36.9	53	68
	51.5	77	90
Neck	75.1	98	100
	72.9	99	100
	59.7	88	94
	54.9	79	79
Wrist	43.2	65	71
	26.5	47	59
	51.8	76	78
	15.1	39	52

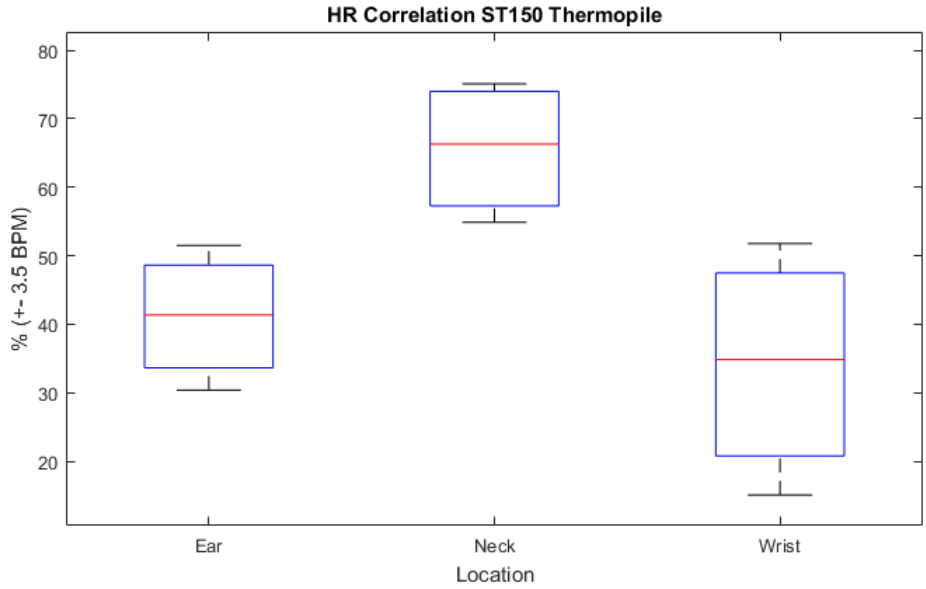

Figure 5.12: Boxplot of the correlation percentages based on the location with a 3.5 BPM range for the ST150

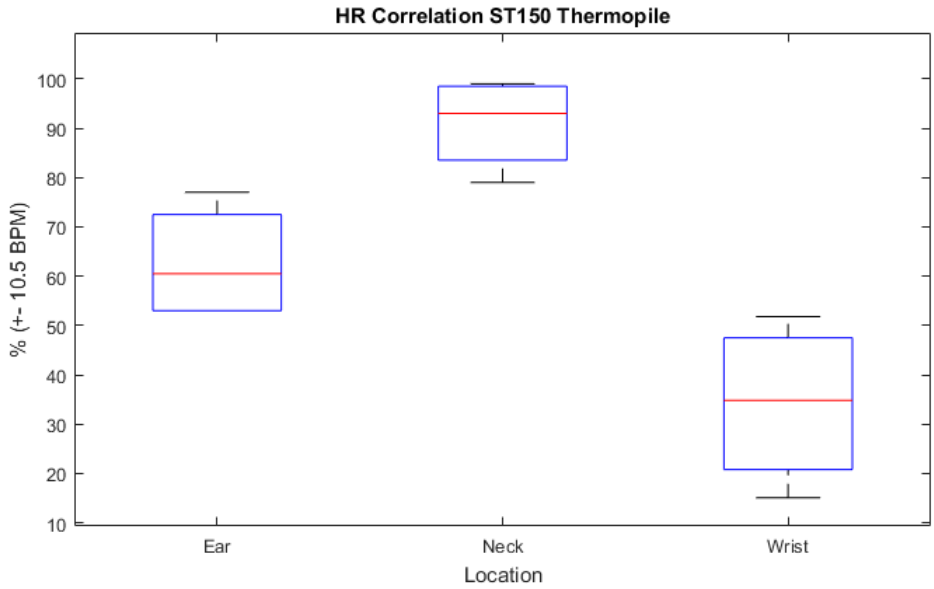

Figure 5.13: Boxplot of the correlation percentages based on the location with a 10.5 BPM range for the ST150

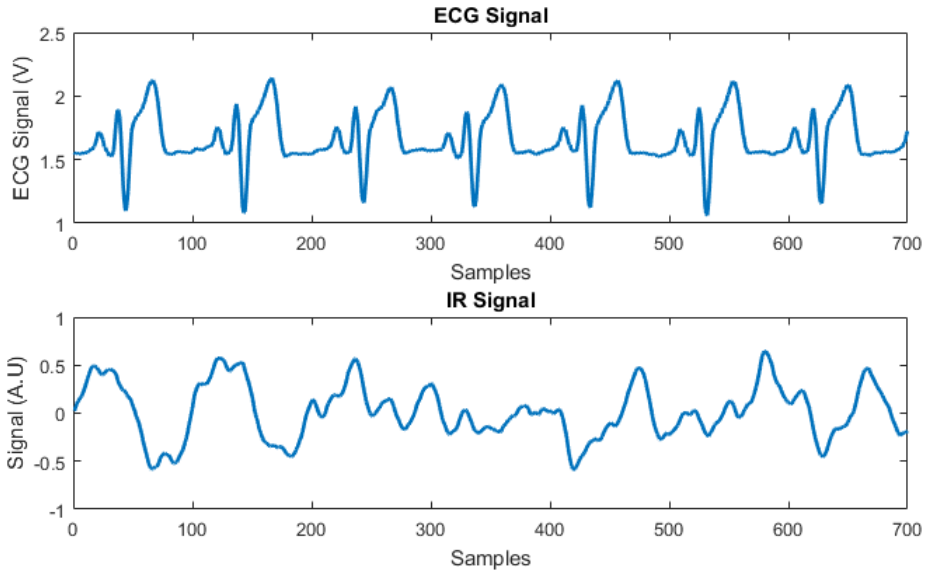

Figure 5.14: Excerpt of the output of the ZTP-135SR and corresponding ECG signal of a sample in the ear

Figure 5.14 shows an excerpt of a signal taken from location A (Cavum conchae) with the fan turned on. This measurement was one of the results with better performance and it is possible to see good heat waveform profiles at the beginning and the end of the sample. However, in the middle of the sample, it is also very clear a reduction in signal quality as the peak from the heat signal are not in the same amplitude or frequency as the ECG.

The resulting CWT analysis of the signal is congruent with this as the correlation is strong in some time slots but a lot of signal corruption is still visible. Figure 5.15 shows the CWT analysis and figure 5.16 shows the corresponding maximum coefficient calculation of the sample.

Figure 5.17 shows the boxplot of the distribution of samples for the 4 treatments for the first range. Figure 5.18 shows the distribution of correlation percentage for the second range. In the figures, it is clear that the medians of the distributions are not very different and the correlation values are not very high. The effect of the fan does not affect the median of the locations and does not help to detect the heart rate.

By taking the whole group of locations A and B, the comparison of the best location was done. The boxplots in figure 5.19 and figure 5.20 show the distribution for all A and B locations including the fan treatments. The B location presents less scattering of the distribution and higher mean in the second range, but location A has better maximums than location B. This could mean that location A has a better bioheat transfer signal but it is more difficult to find with the positioning of the sensors this would explain the big dispersion of data in position A. Nevertheless, the correlation percentage of both positions is very low and do not give reliable heart rate information.

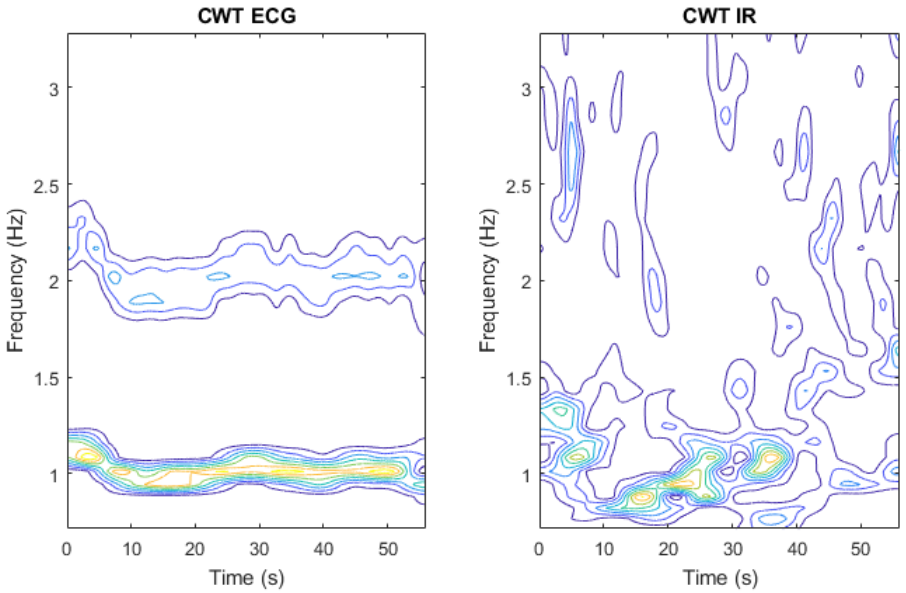

Figure 5.15: Contour plot of CWT coefficients of the ECG signal and the ZTP-135SR signal from a sample in the ear

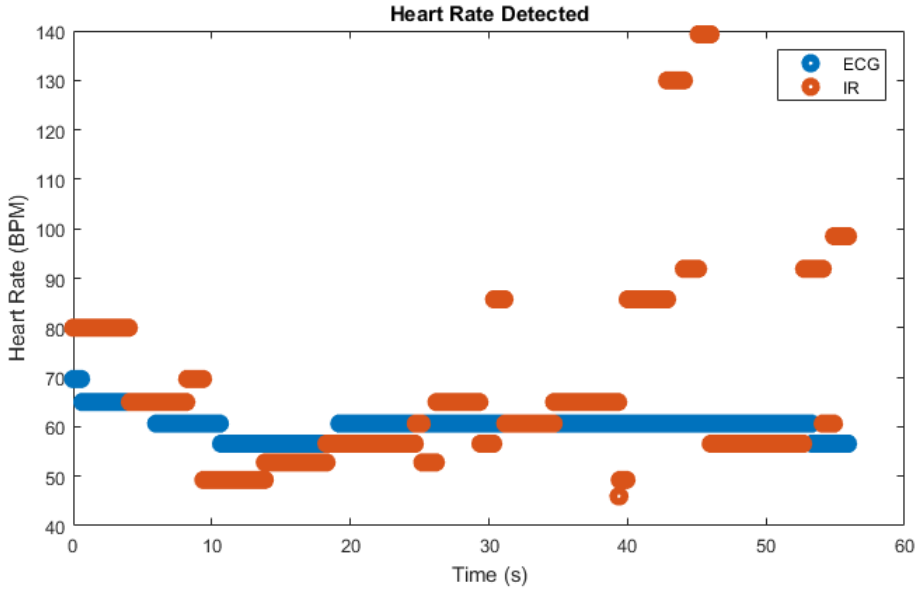

Figure 5.16: Heart rate detected from the ZTP-135SR signal (Orange) and ECG signal (Blue) from a sample in the ear

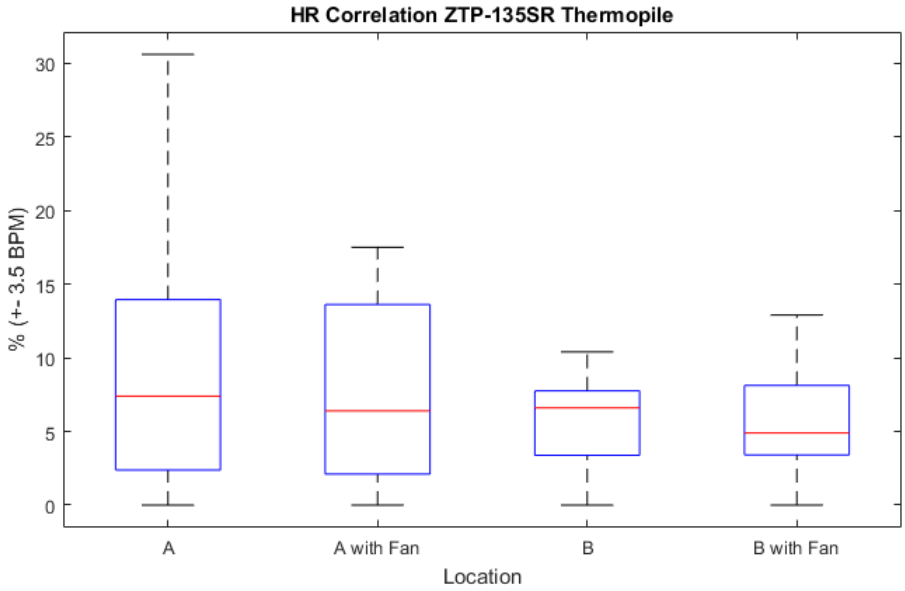

Figure 5.17: Boxplot of the correlation percentages based on the 4 treatments with a 3.5 BPM range for the ZTP-135SR

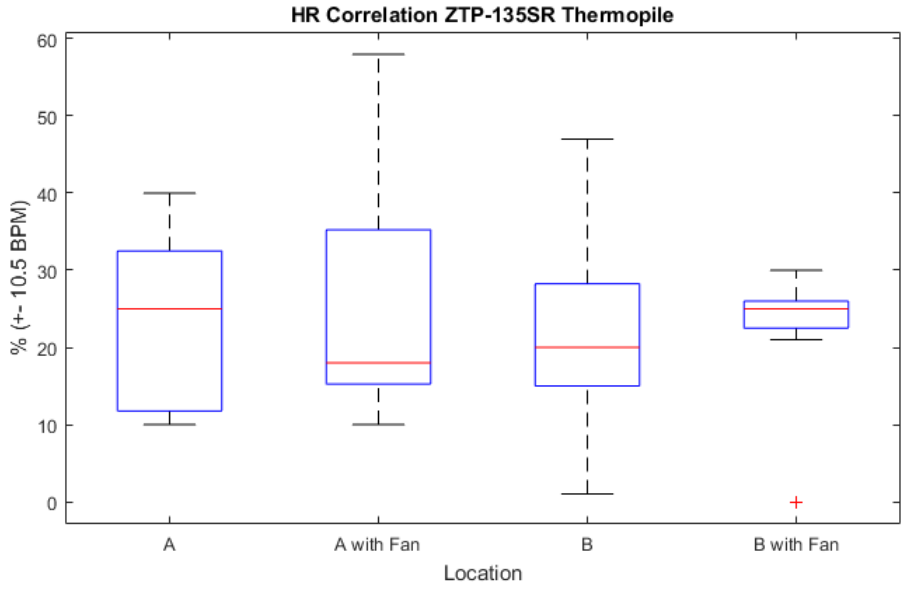

Figure 5.18: Boxplot of the correlation percentages based on the 4 treatments with a 10.5 BPM range for the ZTP-135SR

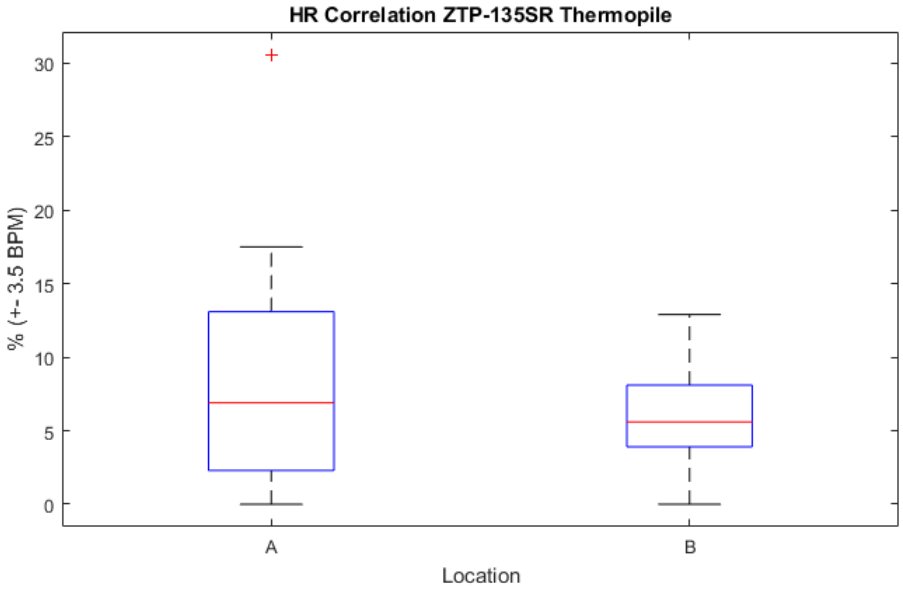

Figure 5.19: Boxplot of the correlation percentages based only on the location with a 3.5 BPM range for the ZTP-135SR

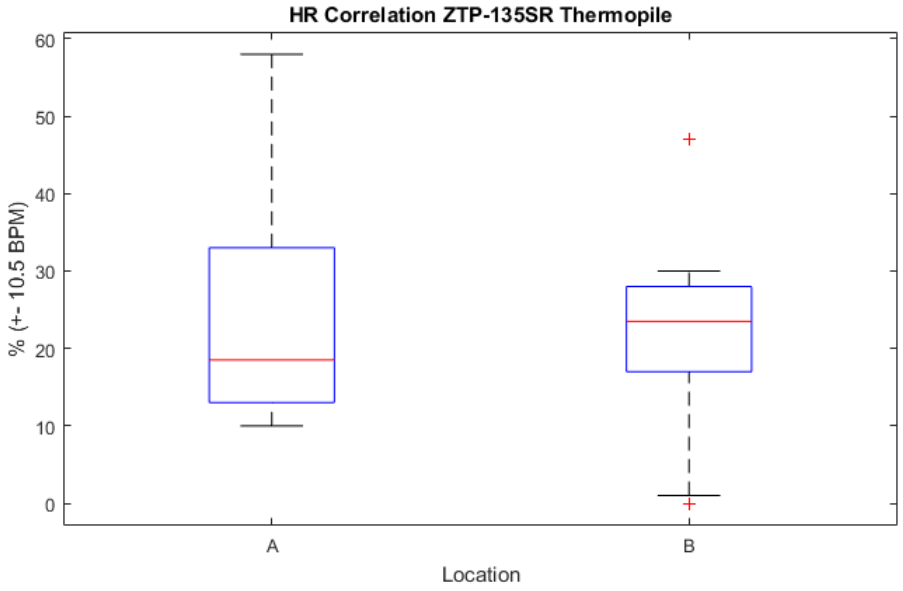

Figure 5.20: Boxplot of the correlation percentages based only on the location with a 10.5 BPM range for the ZTP-135SR

5.5. TO-5 Size

The final tests were performed using the ST150 thermopile exclusively in the ear. The tests compared the close range measurements to ones with a separation of 1 cm between the skin and the sensor. The separation treatment has significantly larger mean than the close range treatment in both error ranges. The distance increases the exposed area of the skin to the sensor and subsequently improves the ability of the system to see pulsating heat exchange.

While the results gathered from this test are not as clear as the signals from the neck, the results are significantly larger than all the previous results in the ear. Figure 5.21 shows an excerpt of a signal from a distance of 1 cm. The waveform of the signal has clearly defined peaks at the same sample times of the ECG peaks but some of them present additional smaller peaks in between. This behavior generates noise in the higher frequency range as it is possible to see in the CWT analysis presented in figure 5.22.

Still, the extraction of the corresponding heart rate from the CWT is considerably similar to the ECG measurements. The results are shown in figure 5.23 in blue representation for the ECG and orange representation for the IR.

Figure 5.24 shows the correlation percentage of the two distances at the first error range, while figure 5.25 shows the percentage at the 10.5 BPM range. The results show that the median of the measurement results taken from a 1 cm distance are significantly better than taken from close range.

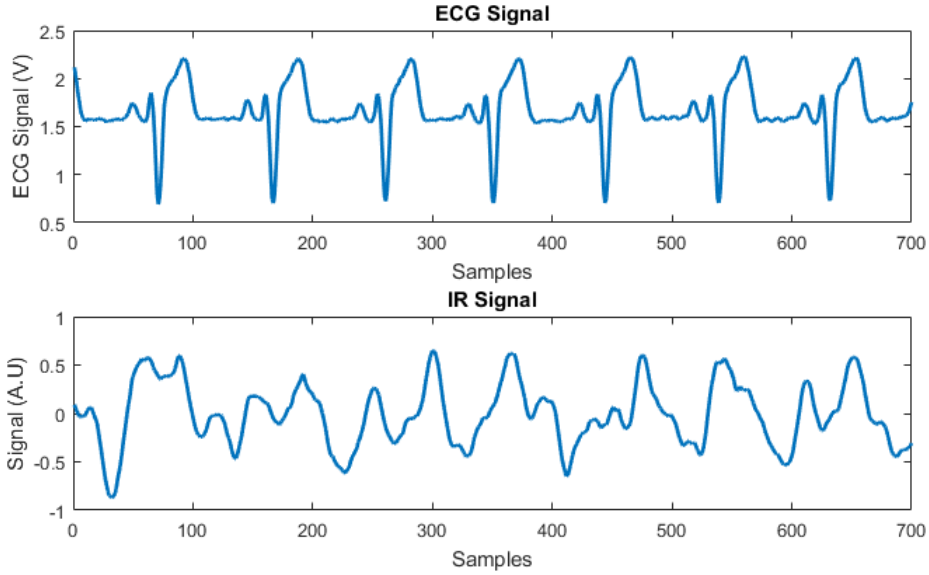

Figure 5.21: Excerpt of the output of the ST150 and corresponding ECG signal of a sample in the ear at 1 cm separation

As a comparison, the results of all the ear measurements done were compiled using both of the error ranges. The results are shown in figure 5.26 for the first range and in figure 5.27 for the second. The results show that the digital sensor was the most unreliable followed by the small TO46 sensor. The correlation coefficient, for the range of ±10.5 BPM, that was calculated for the digital sensor did not surpassed 20% of correlation while the small sensor had 25% of the values above 30%. The sensor that had the strongest signal

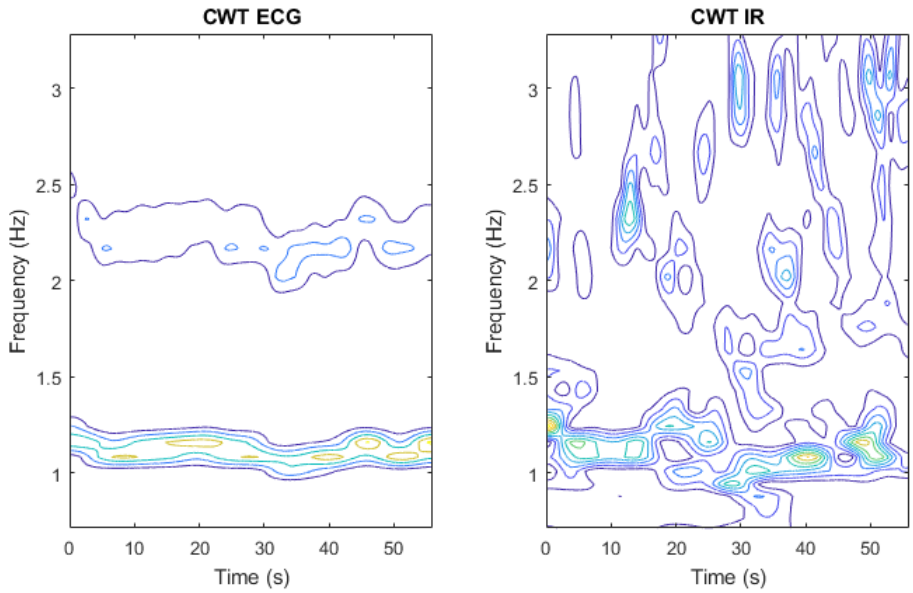

Figure 5.22: Contour plot of CWT coefficients of the ECG signal and the ST150 signal from a sample in the ear at 1 cm separation

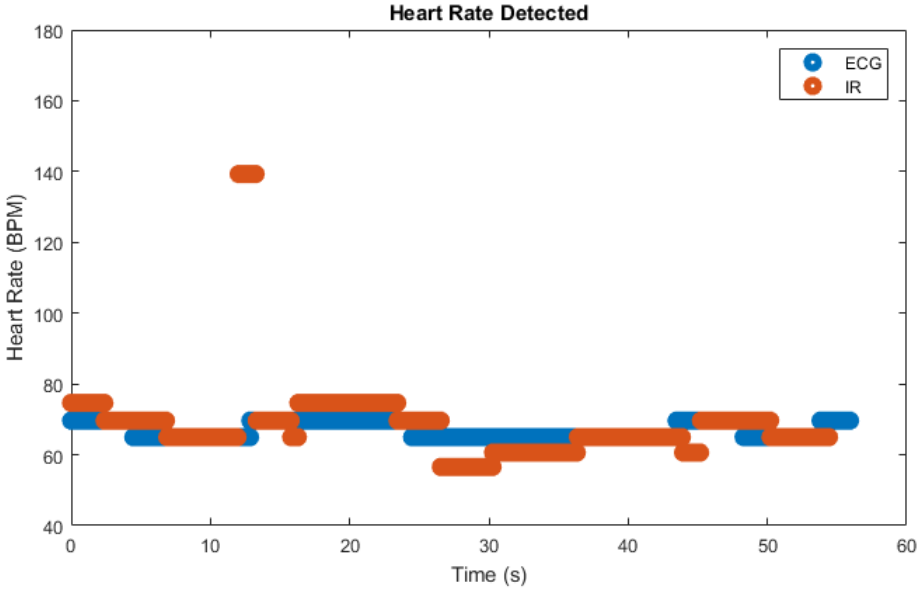

Figure 5.23: Heart rate detected from the ST150 signal (Orange) and ECG signal (Blue) from a sample in the ear at 1 cm separation

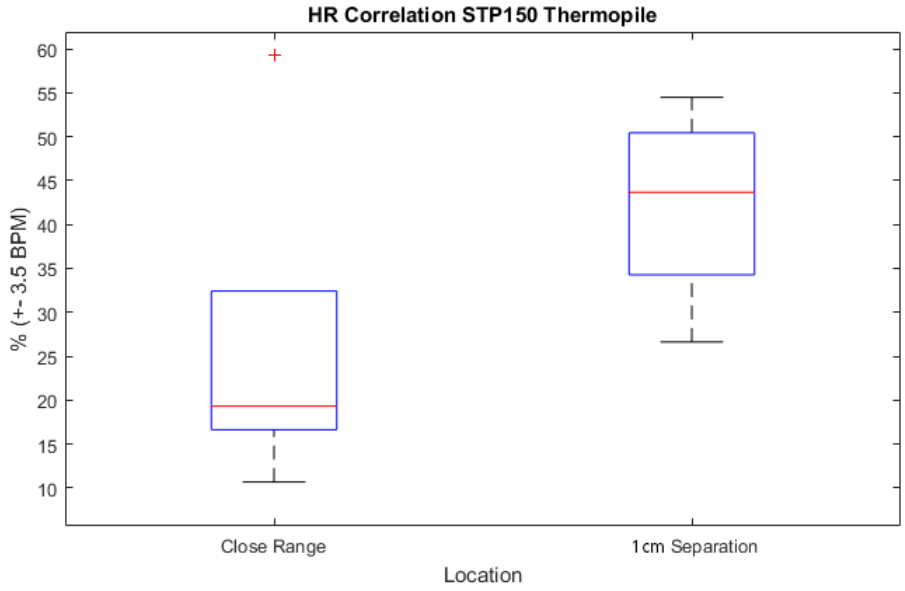

Figure 5.24: Boxplot of the correlation percentages based on the separation distance with a 3.5 BPM range for the ST150

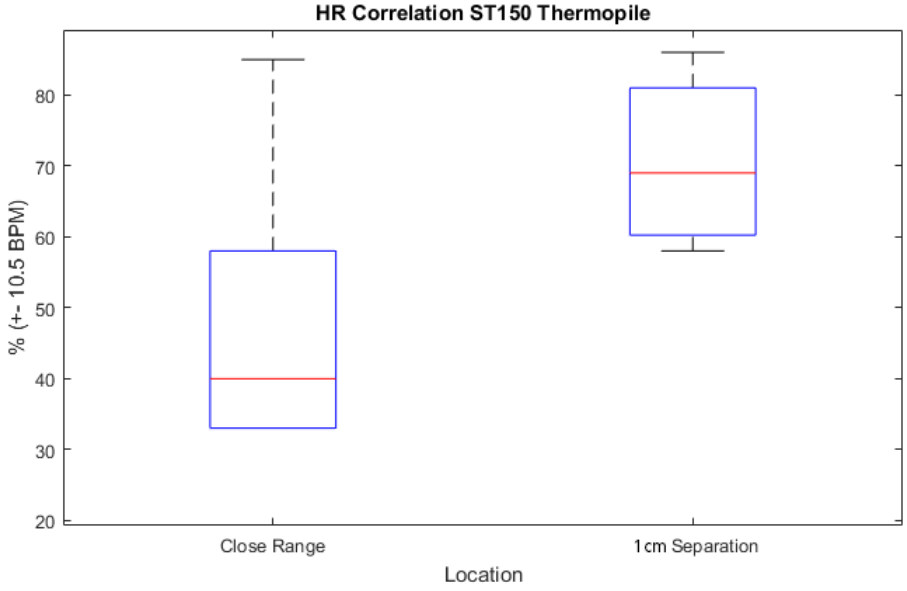

Figure 5.25: Boxplot of the correlation percentages based on the separation distance with a 10.5 BPM range for the ST150

output was the TO5 ST150. In the last measurements, the results were considerably higher than the other ear measurements and relativity close to neck measurements. Out of all the measurements, half of the measurements had a correlation coefficient between 70% and 90%.

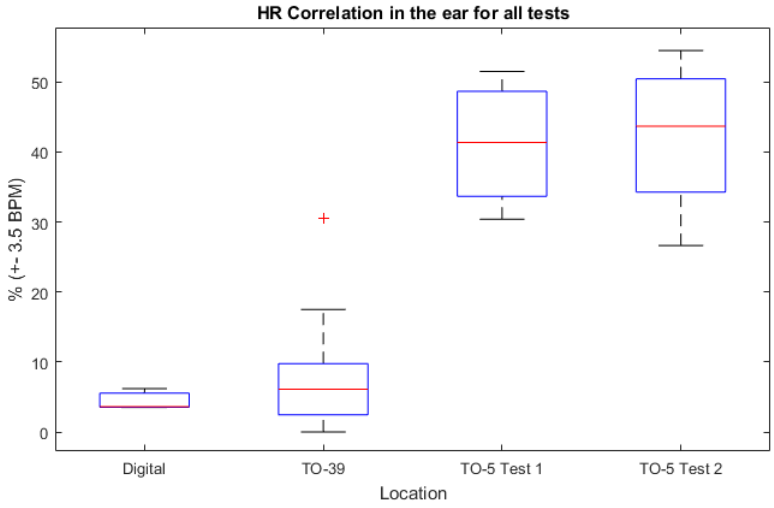

Figure 5.26: Boxplot of the correlation percentages based only ear measurements with a 3.5 BPM range for all sensors

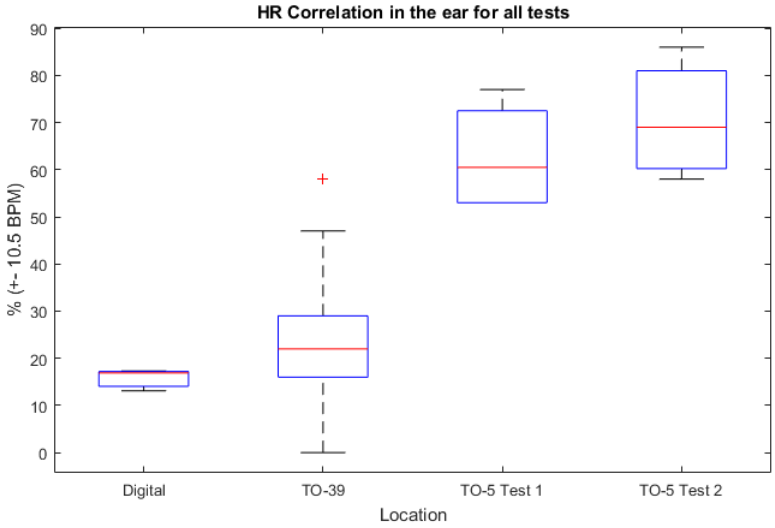

Figure 5.27: Boxplot of the correlation percentages based only ear measurements with a 10.5 BPM range for all sensors

6

Conclusion

A comprehensive analysis of the existing methodologies for extraction of heart rate was performed, after considering the requirements of the project, infrared thermometry was selected as the most promising technique taking into account that the development of PPG technology has slowed down. The bioheat transfer theory from the core of the body to the skin through the blood was analyzed. The inner ear canal was discarded from measurement due to the lack of heat dissipation to the environment required for the measurements. The external ear was selected as the location with the larger heat dissipation. The arterial distribution of the external ear was researched in order to find the location that had the best blood irrigation. The cavum conchae and the antitragus were selected based on that they serve as entry points for the posterior auricular artery and the superficial temporal artery.

The digital sensor MLX96015 that was first tested, was highly affected by quantization noise, causing unwanted peaks on the infrared signal. The resolution of the sensor was capped by the signal processing system of the sensor, with no feasible modifications to improve the signal. The detected heart rate with this sensor was lower than 10% of correlation percentage in the measurements taken in the ear, neck, nose and wrist. This lead to the use of analog sensors in which the amplifier circuit was customizable. Subsequently, a test was done to measure the NETD of the sensor at the usual temperatures of the human body. Responsivity and noise were recorded using a set-up that consisted of a peltier cooler and a pt100 sensor. The NETD calculated was 52 mk and was used as reference point for future measurements.

The physical localization of the sensor is of key importance for this application, during the measurements of the bioheat transfer, it was hypothesized that the localization of the arteries will influence strongly the signal to noise ratio of the signal. However, the 2 locations that were analyzed did not give significant results due to the size of the sensor. The active area of the sensor and the separation from the skin are strongly related to the signal quality of the heart rate signal. In both locations evaluated, the sensor was placed very close to the skin and this was unfavorable since the detected skin area was narrowed and the amount of heat dissipation was reduced.

In order to improve the signal, measurements were made with the sensor separated a distance of 1 cm from the skin. The results confirmed that when the distance increased,

the heart rate components of the signal also increased. This occurs because the separation increases the skin area that emits radiation onto the sensor. The field of view of the sensor can also be modified and this will aid the detection of the artery heat profile by increasing further the detection area.

The energy consumption of the system is another essential characteristic. The system only needs to implement an amplifier for the output and the sensor produces its own voltage and do not require a power source. PPG based systems require a light source and a detector in order to measure heart rate. This is one of the major contributions that this technology could do to the heart rate measurement devices, since the reduction of power consumption is crucial on wearable applications where low power consumption could be translated into a significant increase in the amount of hours that the heart rate of the user can be monitored.

Given that the bioheat transfer is not an instantaneous phenomenon, the rate of heat transfer acts as filter for high frequencies. It was found that the slow movements of the heat through the tissue (Compared to electrical signals) reduce the signal strength when pulse frequency increases, this means that the sensor will decrease its resolution when the heart rate is increased which happens during exercise. Applications for sports settings become very challenging but other applications are interesting.

An intriguing application for the continuous measurements of heart rate is the monitoring of the cardiovascular system in elderly patients. This population requires continuous monitoring and this technology can be combined with hearing aids to provide a more complete system. The fact that the hearing aids are already implemented in an earpiece can make the implementation of the system fast and comfortable.

The motion artifacts were not addressed in this research. The mechanical support of the sensor needs to be improved further for this to be studied. Preliminary testing on the performance of the signal under motion artifacts show that the motion artifacts are several orders of magnitude higher than the heart rate signal. This is the first approach for infrared thermometry in the ear for heart rate extraction that is known in literature and the possibilities for wearable applications are promising based on the successful results obtained. Future work needs to provide better signal to noise ratio and better sensor localization.

A

Appendix

A.1. ECG front end used

In order to compare IR measurements with the corresponding real heart rate, an ECG control was chosen. By reading the electrical signals of the heart, the heart rate can be extracted by applying only a low pass filter. The peaks of the ECG signal can also be used to point the exact pulses of the heart and the corresponding heat fluctuations in the tissue. Because the ECG signal is instant while the heat transfer requires more time, a time delay between the signals was expected.

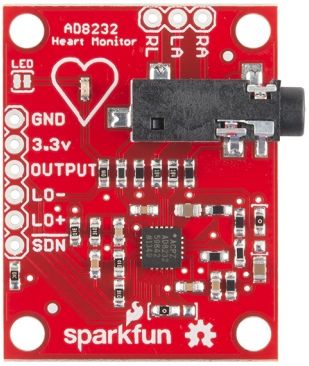

Figure A.1: ECG front-end module used for control measurements

In order to record the physiological signals of the heart, a 3 lead ECG module was implemented. The stand alone module implements an IC from Analog Devices AD8232 and can be seen in figure A.1. This IC is a fully integrated single-lead ECG front end that has been optimized for heart potentials. Because the chip requires a 3.3V source, a LM1117-3.3 linear regulator was used to solve the power requirements.

The ECG module is connected to the electrodes through a 3.5mm audio jack connector. The electrodes are connected to the right side of the upper chest, the left side of the upper chest and the left side of the lower abdomen. To perform the measurements, TIGA-MED AgCL ECG electrodes were used. The electrodes were not reused and were discarded after

each set of measurements.

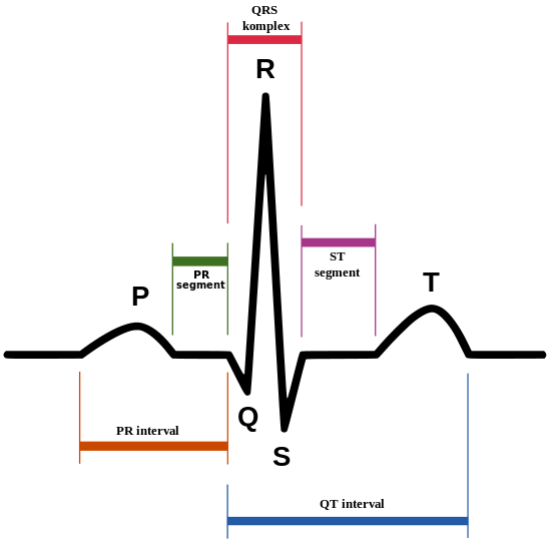

Figure A.2: Standard PQRST complex waveform

The output of the ECG module is an analog output between 0 and 3.3 V. The waveform of the output represent the PQRST shown in figure A.2. While the module is not accurate enough to be able to identify all the PQRST waveforms, the R and T peaks are easily identifiable and are the characteristics used to extract the heart rate.

A.2. Low Noise Amplifier

To limit the noise of the system, two low noise amplifiers were selected. The noise level of the first amplifier used, the OP27, is 80nV in the 0.1-10 Hz range. The noise level of the amplifier is then in the same order of magnitude as the thermopile sensor. In order to further reduce the noise level of the amplifier stage, an ultra-low noise amplifier was implemented later on. The LT1028 implements a noise level of 35 nV in the 0.1-10 Hz range.

A.3. Filter

Due to the frequency nature of the heart beats, it is beneficial to filter out high frequencies. The frequency range of the heart rate signal is comprised between 40-200 beats per minutes (0.66 - 3.33 Hz).

A low pass filter was selected to cut off frequencies higher than 10 Hz. The chip implemented was the LTC1062 with a 5th order filter in a DIP casing and it had no DC error. Additionally, the filter operates at a dual supple of 8 Volts which was then selected as the supply voltage for the other circuits including the signal acquisition module.

A.4. Signal Acquisition

To read the analog voltage of the thermopile after amplification, an analog to digital converter was used. The device chosen was the USB 6210 from National Instruments which implements 8 differential channels. The device has a maximum resolution of 50 ns and is shown in figure A.3. The ADC resolution is 16 bits and it was linked with a PC and the data was saved using MATLAB. The maximum working voltage was 10 V but it was the voltage was limited to 8 V due to the requirements of the low pass filter.

Figure A.3: NI USB 6210 used to acquire the analog signals from the ECG and the IR sensor

A.5. PCB Layout

The design of the board was made in Altium using 2 layers. The front side of the PCB is shown on Figure A.5 and poses the main integrated circuits. The board can select a DIP8 amplifier or a SOIC amplifier using jumpers. It also implements an optional signal follower. The board is located inside an insulated box in order to reduce 50 Hz noise in the preamplifier stage. The board is 58.42 mm wide and 37.85 mm high and was fabricated using FR-4 TG130 material by Seeedstudio. The thickness of the PCB is 1.6 mm, the surface has a Hot Air Solder Level (HASL) finish and a 1 oz copper weight.

Figure A.4 shows the circuit diagram of the whole board. The system implements 2 amplifiers, the 3.3v regulator, the filter and an additional buffer. The optional filter was not used in the measurements but was placed if additional signals wanted to be studied. Figure A.5 shows the front layer of the PCB that contains all the IC's used. Meanwhile, figure A.6 shows the back side that only contains capacitors and resistors. The space was not a limiting factor in this board since it was not required for a completely wearable system.

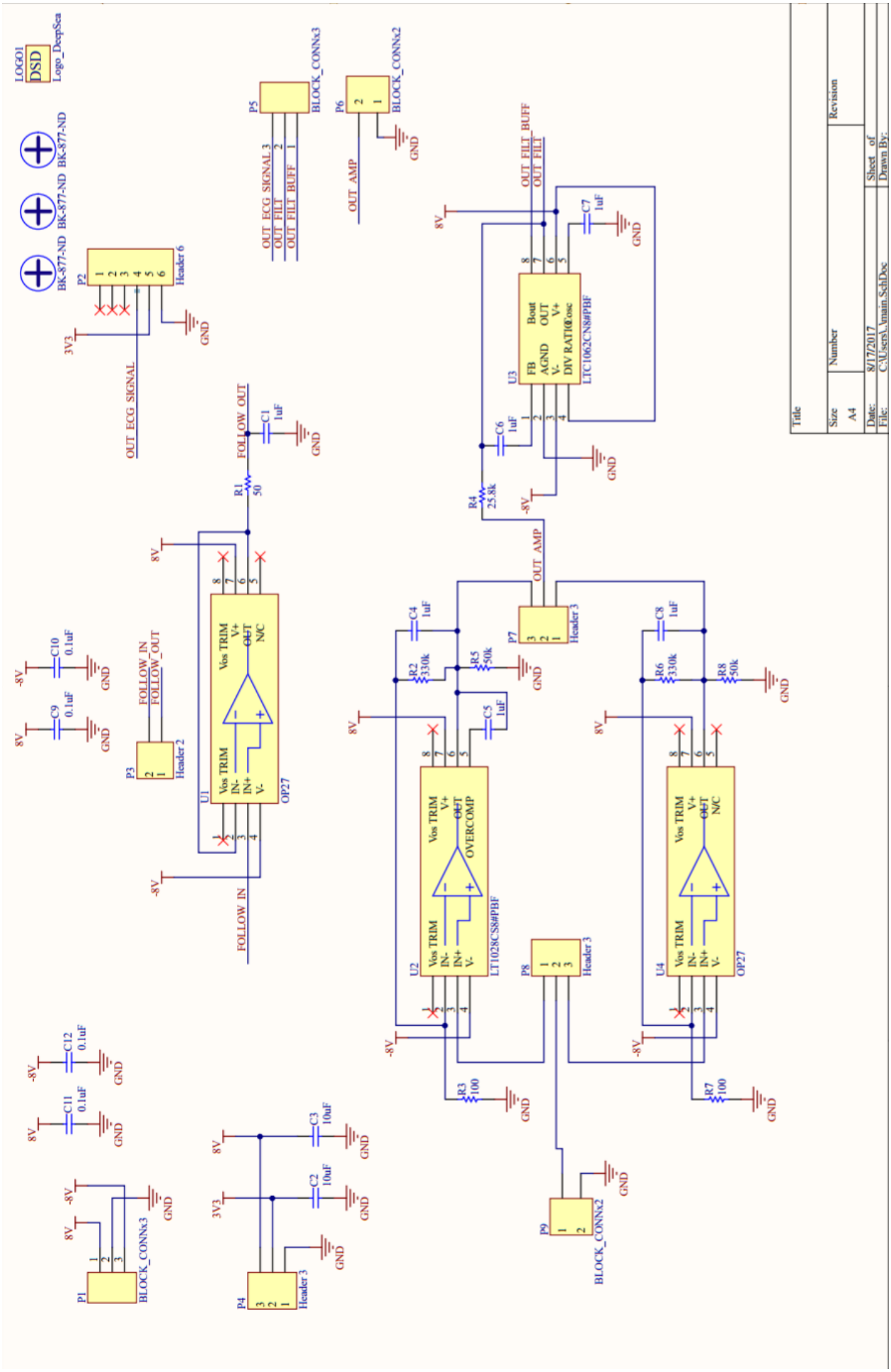

Figure A.4: Circuit Diagram of the complete board

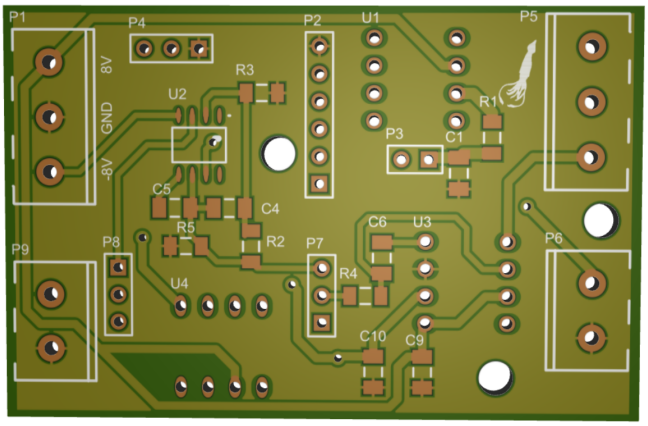

Figure A.5: Front side of the PCB

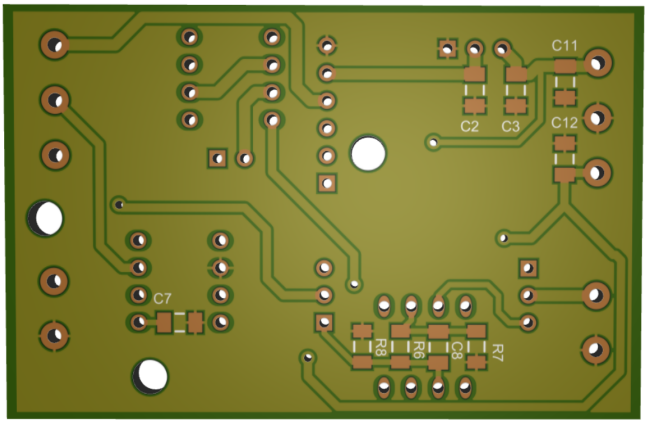

Figure A.6: Back layer of the PCB

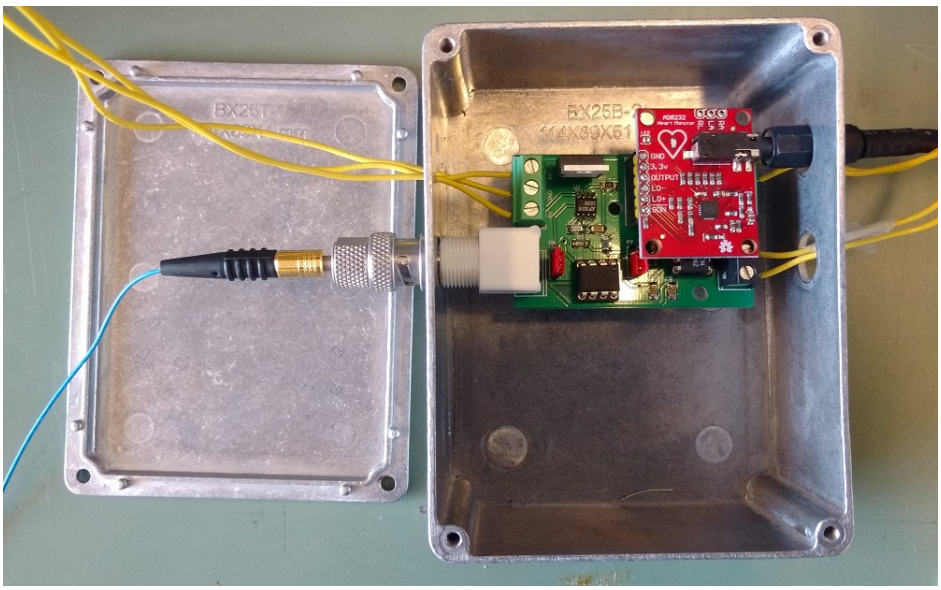

Figure A.7: The shielded system connected with the input (blue coaxial cable) and the ECG module (black cable)

B

Appendix

B.1. MATLAB Code

```
%% Continous Wavelet Analysis and Heart Rate Detection

% Import data
A=importdata('05_24_E_N1.mat');
% Trim first and last data points
IR=A(100:end-100,3);
ECG1=A(100:end-100,2);
% Frequency definition
Fs=100;

%% Filter ECG

windowSize = 30;
b = (1/windowSize)*ones(1,windowSize);
a = 1;
ECG = filter(b,a,ECG1);

subplot(4,1,1)
plot(ECG1(2500:3000))
subplot(4,1,2)
plot(ECG(2500:3000))


%% Filter IR
IR=A(100:end-100,1);
IR2=A(100:end-100,1);

windowSize = 120;
window2=windowSize/2;

% Select Visualization Window
win1=2500;
win2=3000;

b = (1/windowSize)*ones(1,windowSize);
a = 1;
```

```
37
38 % Plot normal signal
39 subplot(4,1,3)
40 plot(IR(win1:win2))
41 IR2 = filter(b,a,IR);
42
43 % Plot DC leve
44 hold on
45 plot(IR2(win1+window2:win2+window2))
46 hold off
47
48
49 % Adjust timing and substract DC level
50 IR2=IR2(window2:end);
51 IR2=[IR2;ones(window2-1,1)];
52 IR=IR-IR2;
53
54 % Plot new filtered signal
55 subplot(4,1,4)
56 plot(IR(win1+window2:win2+window2))
57
58 %Trim after Filter
59 IR=IR(200:end-200);
60 ECG=ECG(200:end-200);
61
62 %% CWT calculation
63
64 % Frequency cut off
65 f1=39;
66 f2=61;
67
68 % Calculate CWT
69 figure;
70 subplot(1,2,1)
71 [wt,f,coi]=cwt(ECG,'bump',Fs);
72 y1 = linspace(0,56,length(ECG));
73 y2=abs(wt(f1:f2,:)).^2;
74
75 %  Plot contour figure
76 contour(y1,f(f1:f2),y2);
77
78 % Save maximum values
79 [m1 ma1]=max(y2);
80 axis tight;
81 title('CWT ECG')
82 xlabel('Time (s)')
83 ylabel('Frequency (Hz)')
84
85 % Same procedure for IR signal
86 subplot(1,2,2)
87 [wt,f,coi]=cwt(IR,'bump',Fs);
88 y3=abs(wt(f1:f2,:)).^2;
89 contour(y1,f(f1:f2),y3);
90 [m2 ma2]=max(y3);
91 axis tight;
92 title('CWT IR')
```

```
93 xlabel('Time (s)')
94 ylabel('Frequency (Hz)')
95
96 %% Heart Rate Detection
97
98 figure;
99 maxi1=f(f1:f2)*60;
100 maxi1=maxi1(ma1);
101 plot(y1,maxi1,'o', 'LineWidth',4);
102
103 maxi2=f(f1:f2)*60;
104 maxi2=maxi2(ma2);
105 hold on
106 plot(y1,maxi2,'o', 'LineWidth',4);
107 legend('ECG','IR')
108 title('Heart Rate Detected')
109 xlabel('Time (s)')
110 ylabel('Heart Rate (BPM)')
111 hold off
112
113 % Correlation coefficients calculation
114 mcomp=abs(ma1-ma2);
115 comp0=sum(mcomp==0);
116 comp1=sum(mcomp<2);
117 comp2=sum(mcomp<3);
118 comp3=sum(mcomp<4);
119 total=length(ma1);
120 asdf=(comp0/total)*100;
121 asdf2=(comp1/total)*100;
122
123 mcompa=[comp0,comp1,comp2,comp3,total, f(f1), f(f2),...
124     (comp0/total)*100,(comp1/total)*100,(comp2/total)*100,(comp3/total)*100 ...
        ]
125 % close all
```

Bibliography

[1] Amirhosein Khas Ahmadi, Parsa Moradi, Mahan Malihi, Sajjad Karimi, and Mohammad B. Shamsollahi. Heart Rate monitoring during physical exercise using wrist-type photoplethysmographic (PPG) signals. In *Engineering in Medicine and Biology Society (EMBC), 2015 37th Annual International Conference of the IEEE*, pages 6166–6169. IEEE, 2015. URL http://ieeexplore.ieee.org/abstract/document/7319800/.

[2] Majd AlGhatrif and Joseph Lindsay. A brief review: history to understand fundamentals of electrocardiography. *Journal of Community Hospital Internal Medicine Perspectives*, 2(1), April 2012. ISSN 2000-9666. doi: 10.3402/jchimp.v2i1.14383. URL http://www.jchimp.net/index.php/jchimp/article/view/14383.

[3] Robert Amelard, David A. Clausi, and Alexander Wong. Spectral photoplethysmographic imaging sensor fusion for enhanced heart rate detection. page 970113, March 2016. doi: 10.1117/12.2213687. URL http://proceedings.spiedigitallibrary.org/proceeding.aspx?doi=10.1117/12.2213687.

[4] Amir Mohammad Amiri, Giuliano Armano, Amir Mohammad Rahmani, and Kunal Mankodiya. PhonoSys: Mobile Phonocardiography Diagnostic System for Newborns. ICST, 2015. ISBN 978-1-63190-088-4. doi: 10.4108/eai.14-10-2015.2261614. URL http://eudl.eu/doi/10.4108/eai.14-10-2015.2261614.

[5] K Barnes, V Kauffman, and C Connolly. Health wearables: Early days, 2014. URL www.pwc.com/us/healthindustries.

[6] Arka Bhowmik, Rupesh Singh, Ramjee Repaka, and Subhash C. Mishra. Conventional and newly developed bioheat transport models in vascularized tissues: A review. *Journal of Thermal Biology*, 38(3):107–125, April 2013. ISSN 03064565. doi: 10.1016/j.jtherbio.2012.12.003. URL http://linkinghub.elsevier.com/retrieve/pii/S0306456512001659.

[7] Olaf Binsch, Thymen Wabeke, and Pierre Valk. Comparison of three different physiological wristband sensor systems and their applicability for resilience-and work load monitoring. In *Wearable and Implantable Body Sensor Networks (BSN), 2016 IEEE 13th International Conference on*, pages 272–276. IEEE, 2016. URL http://ieeexplore.ieee.org/abstract/document/7516272/.

[8] Laura Boccanfuso, Eva Juarez Perez, Myra Robinson, and Jason M. O'Kane. Collecting heart rate using a high precision, non-contact, single-point infrared temperature sensor. In *International Conference on Social Robotics*, pages 86–97. Springer, 2012. URL http://link.springer.com/chapter/10.1007/978-3-642-34103-8_9.

[9] Gavriloaia Bogdan, Vizireanu Radu, Fratu Octavian, Berechet Alin, Mara Constantin, and Cucu Cristian. Remote assessment of heart rate by skin color processing. In

Communications and Networking (BlackSeaCom), 2015 IEEE International Black Sea Conference on, pages 112–116. IEEE, 2015. URL http://ieeexplore.ieee.org/abstract/document/7185097/.

[10] Ilaria Bosi, Chiara Cogerino, and Marco Bazzani. Real-time monitoring of heart rate by processing of Microsoft Kinect™ 2.0 generated streams. In *Computer and Energy Science (SpliTech), International Multidisciplinary Conference on*, pages 1–6. IEEE, 2016. URL http://ieeexplore.ieee.org/abstract/document/7555944/.

[11] D Bothun and M Lieberman. The Wearable Life 2.0, 2016. URL pwc.com/CISwearables.

[12] Dilpreet Buxi, Julien Penders, and Chris Van Hoof. Early results on wrist based heart rate monitoring using mechanical transducers. In *Engineering in Medicine and Biology Society (EMBC), 2010 Annual International Conference of the IEEE*, pages 4407–4410. IEEE, 2010. URL http://ieeexplore.ieee.org/abstract/document/5627129/.

[13] Xi Cai, Guang Han, and Jinkuan Wang. Video-based noncontact heart rate measurement using ear features. In *Progress in Informatics and Computing (PIC), 2015 IEEE International Conference on*, pages 262–265. IEEE, 2015. URL http://ieeexplore.ieee.org/abstract/document/7489850/.

[14] Madhurima Chattopadhyay and Debjyoti Chowdhury. Design and performance analysis of MEMS capacitive pressure sensor array for measurement of heart rate. *Microsystem Technologies*, February 2016. ISSN 0946-7076, 1432-1858. doi: 10.1007/s00542-016-2842-2. URL http://link.springer.com/10.1007/s00542-016-2842-2.

[15] Sergei Churkin and Lesya Anishchenko. Millimeter-wave radar for vital signs monitoring. In *Microwaves, Communications, Antennas and Electronic Systems (COMCAS), 2015 IEEE International Conference on*, pages 1–4. IEEE, 2015. URL http://ieeexplore.ieee.org/abstract/document/7360366/.

[16] Oana I. Craciunescu and Scott T. Clegg. Pulsatile Blood Flow Effects on Temperature Distribution and Heat Transfer in Rigid Vessels. *Journal of Biomechanical Engineering*, 123(5):500, 2001. ISSN 01480731. doi: 10.1115/1.1392318. URL http://Biomechanical.asmedigitalcollection.asme.org/article.aspx?articleid=1406579.

[17] A. Cuadras and O. Casas. Determination of heart rate using a high-resolution temperature measurement. *IEEE Sensors Journal*, 6(3):836–843, June 2006. ISSN 1530-437X. doi: 10.1109/JSEN.2006.874445. URL http://ieeexplore.ieee.org/document/1634437/.

[18] Angel Cuadras and S. Casas. High resolution temperature measurement [biomedical applications]. In *Sensors, 2004. Proceedings of IEEE*, pages 1363–1368. IEEE, 2004. URL http://ieeexplore.ieee.org/abstract/document/1426437/.

[19] Yang Cui, Chang-Hong Fu, Hong Hong, Yijin Zhang, and Feng Shu. Non-contact time varying heart rate monitoring in exercise by video camera. In *Wireless Communications & Signal Processing (WCSP), 2015 International Conference on*, pages 1–5. IEEE, 2015. URL http://ieeexplore.ieee.org/abstract/document/7341278/.

[20] D. Feng. *Heart Rate Variability Analysis Based on Instantaneous Frequency Estimation*. PhD thesis, TU Delft, Delft University of Technology, 2015. URL http://repository.tudelft.nl/assets/uuid:d7b9c340-b21f-41a2-a723-3904478190b4/Heart_Rate_Variability_Analysis_Based_on_Instantaneous_Frequency_Estimation_Di_Feng.pdf.

[21] Fran??Ois Xavier Gamelin, Serge Berthoin, and Laurent Bosquet. Validity of the Polar S810 Heart Rate Monitor to Measure R-R Intervals at Rest:. *Medicine & Science in Sports & Exercise*, 38(5):887–893, May 2006. ISSN 0195-9131. doi: 10.1249/01.mss.0000218135.79476.9c. URL http://content.wkhealth.com/linkback/openurl?sid=WKPTLP:landingpage&an=00005768-200605000-00013.

[22] P Silva Girão, O Postolache, G Postolache, P M Ramos, and J M Dias Pereira. Microwave Doppler radar in unobtrusive health monitoring. *Journal of Physics: Conference Series*, 588:012046, February 2015. ISSN 1742-6596. doi: 10.1088/1742-6596/588/1/012046. URL http://stacks.iop.org/1742-6596/588/i=1/a=012046?key=crossref.4974287db0b7f1089620ce3ef0692b35.

[23] Jeffrey L. Goodie, Kevin T. Larkin, and Scott Schauss. Validation of the Polar Heart Rate Monitor for Assessing Heart Rate During Physical and Mental Stress. *Journal of Psychophysiology*, 14(3):159–164, July 2000. ISSN 0269-8803, 2151-2124. doi: 10.1027//0269-8803.14.3.159. URL http://econtent.hogrefe.com/doi/abs/10.1027//0269-8803.14.3.159.

[24] Kian Hamedani, Zahra Bahmani, and Amin Mohammadian. Spatio-temporal filtering of thermal video sequences for heart rate estimation. *Expert Systems with Applications*, 54:88–94, July 2016. ISSN 09574174. doi: 10.1016/j.eswa.2016.01.022. URL http://linkinghub.elsevier.com/retrieve/pii/S0957417416000324.

[25] Mohamed Abul Hassan, Garnir S. Malik, N. Saad, Babak Karasfi, Yasir Salih Ali, and D. Fofi. Optimal source selection for image photoplethysmography. In *Instrumentation and Measurement Technology Conference Proceedings (I2MTC), 2016 IEEE International*, pages 1–5. IEEE, 2016. URL http://ieeexplore.ieee.org/abstract/document/7520406/.

[26] David Da He, Eric S. Winokur, and Charles G. Sodini. An Ear-Worn Vital Signs Monitor. *IEEE Transactions on Biomedical Engineering*, 62(11):2547–2552, November 2015. ISSN 0018-9294, 1558-2531. doi: 10.1109/TBME.2015.2459061. URL http://ieeexplore.ieee.org/document/7163528/.

[27] Kan Hong and Sheng Hong. Real-time stress assessment using thermal imaging. *The Visual Computer*, 32(11):1369–1377, November 2016. ISSN 0178-2789, 1432-2315. doi: 10.1007/s00371-015-1164-1. URL http://link.springer.com/10.1007/s00371-015-1164-1.

[28] Edward Jo, Kiana Lewis, Dean Directo, Michael J. Kim, and Brett A. Dolezal. Validation of Biofeedback Wearables for Photoplethysmographic Heart Rate Tracking. *Journal of sports science & medicine*, 15(3):540, 2016. URL https://www.ncbi.nlm.nih.gov/pmc/articles/PMC4974868/.

[29] Rafael González Landaeta, O. Casas, and R. Pallàs Areny. Detección de las frecuencias cardiaca y respiratoria mediante una báscula electrónica. In *IV Latin American Congress on Biomedical Engineering 2007, Bioengineering Solutions for Latin America Health*, pages 448–451. Springer, 2007. URL http://link.springer.com/chapter/10.1007/978-3-540-74471-9_104.

[30] Dan Ledger. Wearables and the science of human behavior, 2014.

[31] Jonghwa Lee and SeongHwan Cho. A motion-tolerant heart rate detection method using bio-impedance and MUSIC algorithm. In *SENSORS, 2015 IEEE*, pages 1–4. IEEE, 2015. URL http://ieeexplore.ieee.org/abstract/document/7370671/.

[32] Ryan T. Li, Scott R. Kling, Michael J. Salata, Sean A. Cupp, Joseph Sheehan, and James E. Voos. Wearable performance devices in sports medicine. *Sports health*, 8(1):74–78, 2016. URL http://journals.sagepub.com/doi/abs/10.1177/1941738115616917.

[33] Wei-Jheng Lin and Hsi-Pin Ma. A physiological information extraction method based on wearable PPG sensors with motion artifact removal. In *Communications (ICC), 2016 IEEE International Conference on*, pages 1–6. IEEE, 2016. URL http://ieeexplore.ieee.org/abstract/document/7511485/.

[34] Joseph Lounana, Frederic Campion, Timothy D. Noakes, and Jean Medelli. Relationship between %HRmax, %HR Reserve, %V??O2max, and %V??O2 Reserve in Elite Cyclists:. *Medicine & Science in Sports & Exercise*, 39(2):350–357, February 2007. ISSN 0195-9131. doi: 10.1249/01.mss.0000246996.63976.5f. URL http://content.wkhealth.com/linkback/openurl?sid=WKPTLP:landingpage&an=00005768-200702000-00018.

[35] Katy Lydon, Bo Yu Su, Licet Rosales, Moein Enayati, K. C. Ho, Marilyn Rantz, and Marjorie Skubic. Robust heartbeat detection from in-home ballistocardiogram signals of older adults using a bed sensor. In *Engineering in Medicine and Biology Society (EMBC), 2015 37th Annual International Conference of the IEEE*, pages 7175–7179. IEEE, 2015. URL http://ieeexplore.ieee.org/abstract/document/7320047/.

[36] Y. Maeda, M. Sekine, T. Tamura, A. Moriya, T. Suzuki, and K. Kameyama. Comparison of reflected green light and infrared photoplethysmography. In *Engineering in Medicine and Biology Society, 2008. EMBS 2008. 30th Annual International Conference of the IEEE*, pages 2270–2272. IEEE, 2008. URL http://ieeexplore.ieee.org/abstract/document/4649649/.

[37] Yuka Maeda, Masaki Sekine, and Toshiyo Tamura. The Advantages of Wearable Green Reflected Photoplethysmography. *Journal of Medical Systems*, 35(5):829–834, October 2011. ISSN 0148-5598, 1573-689X. doi: 10.1007/s10916-010-9506-z. URL http://link.springer.com/10.1007/s10916-010-9506-z.

[38] Marc Mateu-Mateus, Federico Guede-Fernández, and Miguel Angel García-González. RR Time Series Comparison Obtained by H7 Polar Sensors or by Photoplethysmography Using Smartphones: Breathing and Devices Influences. In Igor Lacković and Darko Vasic, editors, *6th European Conference of the International Federation for Medical and Biological Engineering*, volume 45, pages 264–267. Springer International Publishing, Cham, 2015. ISBN 978-3-319-11127-8 978-3-319-11128-5. URL http://link.springer.com/10.1007/978-3-319-11128-5_66.

[39] Mark Melnykowycz, Michael Tschudin, and Frank Clemens. Piezoresistive Soft Condensed Matter Sensor for Body-Mounted Vital Function Applications. *Sensors*, 16(3): 326, March 2016. ISSN 1424-8220. doi: 10.3390/s16030326. URL http://www.mdpi.com/1424-8220/16/3/326.

[40] Aditi Misra, Rohan Banerjee, Anirban Dutta Choudhury, Aniruddha Sinha, and Arpan Pal. Novel peak detection to estimate HRV using Smartphone audio. In *Wearable and Implantable Body Sensor Networks (BSN), 2015 IEEE 12th International Conference on*, pages 1–6. IEEE, 2015. URL http://ieeexplore.ieee.org/abstract/document/7299378/.

[41] George T. Nager and M. Nager. LXXXIII The Arteries of the Human Middle Ear, with Particular Regard to the Blood Supply of the Auditory Ossicles. *Annals of Otology, Rhinology & Laryngology*, 62(4):923–949, 1953. URL http://journals.sagepub.com/doi/pdf/10.1177/000348945306200401.

[42] Nishime E, Cole CR, Blackstone EH, Pashkow FJ, and Lauer MS. Heart rate recovery and treadmill exercise score as predictors of mortality in patients referred for exercise ecg. *JAMA*, 284(11):1392–1398, September 2000. ISSN 0098-7484. doi: 10.1001/jama.284.11.1392. URL http://dx.doi.org/10.1001/jama.284.11.1392.

[43] V Palladino. Hear the pulse: Heart rate monitoring fitness earbuds tested. *arstechnica*, December 2016. URL https://arstechnica.com/gadgets/2016/12/hear-the-pulse-heart-rate-monitoring-fitness-earbuds-tested/.

[44] Jang-Ho Park, Dae-Geun Jang, Jung Park, and Se-Kyoung Youm. Wearable Sensing of In-Ear Pressure for Heart Rate Monitoring with a Piezoelectric Sensor. *Sensors*, 15 (9):23402–23417, September 2015. ISSN 1424-8220. doi: 10.3390/s150923402. URL http://www.mdpi.com/1424-8220/15/9/23402/.

[45] Dung Phan, Lee Yee Siong, Pubudu N. Pathirana, and Aruna Seneviratne. Smartwatch: Performance evaluation for long-term heart rate monitoring. In *Bioelectronics and Bioinformatics (ISBB), 2015 International Symposium on*, pages 144–147. IEEE, 2015. URL http://ieeexplore.ieee.org/abstract/document/7344944/.

[46] Ernesto Serrano-Finetti, Ramon Casanella, Pablo S. Luna-Lozano, and Ramon Pallas-Areny. Unobtrusive Measurement of Heart Rate on a Single Hand by Impedance Plethysmography. In *5th European Conference of the International Federation for Medical and Biological Engineering*, pages 1221–1224. Springer, 2011. URL http://link.springer.com/10.1007/978-3-642-23508-5_316.

[47] Agung Setiabudi, Ryota Sakamoto, Hiroki Tamura, and Koichi Tanno. A Low-Voltage and Low-Power CMOS Temperature Sensor Circuit with Digital Output for Wireless Healthcare Monitoring System. pages 183–188. IEEE, May 2016. ISBN 978-1-4673-9489-5. doi: 10.1109/ISMVL.2016.53. URL http://ieeexplore.ieee.org/document/7515545/.

[48] Chiarella Sforza, Gaia Grandi, Miriam Binelli, Davide G. Tommasi, Riccardo Rosati, and Virgilio F. Ferrario. Age- and sex-related changes in the normal human ear. *Forensic Science International*, 187(1-3):110.e1–110.e7, May 2009. ISSN 03790738. doi: 10.1016/j.forsciint.2009.02.019. URL http://linkinghub.elsevier.com/retrieve/pii/S0379073809000966.

[49] Tsu-Wang Shen, Tim Hsiao, Yu-Tsung Liu, and Tsung-Ying He. An ear-lead ECG based smart sensor system with voice biofeedback for daily activity monitoring. In *TENCON 2008-2008 IEEE Region 10 Conference*, pages 1–6. IEEE, 2008. URL http://ieeexplore.ieee.org/xpls/abs_all.jsp?arnumber=4766645.

[50] Andrew Sherwood, Judy McFetridge, and J. Stanford Hutcheson. Ambulatory impedance cardiography: a feasibility study. *Journal of Applied Physiology*, 85(6):2365–2369, 1998. URL http://jap.physiology.org/content/85/6/2365.short.

[51] Keun-Young Shin, James S. Lee, and Jyongsik Jang. Highly sensitive, wearable and wireless pressure sensor using free-standing ZnO nanoneedle/PVDF hybrid thin film for heart rate monitoring. *Nano Energy*, 22:95–104, April 2016. ISSN 22112855. doi: 10.1016/j.nanoen.2016.02.012. URL http://linkinghub.elsevier.com/retrieve/pii/S221128551600063X.

[52] Yi Shu, Cheng Li, Zhe Wang, Wentian Mi, Yuxing Li, and Tian-Ling Ren. A Pressure sensing system for heart rate monitoring with polymer-based pressure sensors and an anti-interference post processing circuit. *Sensors*, 15(2):3224–3235, February 2015. ISSN 1424-8220. doi: 10.3390/s150203224. URL http://www.mdpi.com/1424-8220/15/2/3224/.

[53] Jayant Sirohi and Inderjit Chopra. Fundamental Understanding of Piezoelectric Strain Sensors. *Journal of Intelligent Material Systems and Structures*, 11(4):246–257, April 2000. ISSN 1045389X. doi: 10.1106/8BFB-GC8P-XQ47-YCQ0. URL http://jim.sagepub.com/cgi/doi/10.1106/8BFB-GC8P-XQ47-YCQ0.

[54] David B. Springer, Thomas Brennan, Jens Hitzeroth, Bongani M. Mayosi, Lionel Tarassenko, and Gari D. Clifford. Robust heart rate estimation from noisy phonocardiograms. In *Computing in Cardiology Conference (CinC), 2014*, pages 613–616. IEEE, 2014. URL http://ieeexplore.ieee.org/abstract/document/7043117/.

[55] David B. Springer, Thomas Brennan, Liesl J. Zuhlke, Hassan Y. Abdelrahman, Ntobeko Ntusi, Gari D. Clifford, Bongani M. Mayosi, and Lionel Tarassenko. Signal quality classification of mobile phone-recorded phonocardiogram signals. In *Acoustics, Speech and Signal Processing (ICASSP), 2014 IEEE International Conference on*, pages 1335–1339. IEEE, 2014. URL http://ieeexplore.ieee.org/abstract/document/6853814/.

[56] Nanfei Sun, Marc Garbey, Arcangelo Merla, and Ioannis Pavlidis. Imaging the cardiovascular pulse. In *Computer Vision and Pattern Recognition, 2005. CVPR 2005. IEEE Computer Society Conference on*, volume 2, pages 416–421. IEEE, 2005. URL http://ieeexplore.ieee.org/abstract/document/1467472/.

[57] Toshiyo Tamura, Yuka Maeda, Masaki Sekine, and Masaki Yoshida. Wearable Photoplethysmographic Sensors—Past and Present. *Electronics*, 3(2):282–302, April 2014. ISSN 2079-9292. doi: 10.3390/electronics3020282. URL http://www.mdpi.com/2079-9292/3/2/282/.

[58] Andriy Temko. Estimation of heart rate from photoplethysmography during physical exercise using wiener filtering and the phase vocoder. In *Engineering in Medicine and Biology Society (EMBC), 2015 37th Annual International Conference of the IEEE*, pages 1500–1503. IEEE, 2015. URL http://ieeexplore.ieee.org/abstract/document/7318655/.

[59] Nitish V. Thakor and Y.-S. Zhu. Applications of adaptive filtering to ECG analysis: noise cancellation and arrhythmia detection. *IEEE transactions on biomedical engineering*, 38(8):785–794, 1991. URL http://ieeexplore.ieee.org/abstract/document/83591/.

[60] Yohei Tomita. Asynchronous noise removal for earbud-based PPG sensors. In *Engineering in Medicine and Biology Society (EMBC), 2016 IEEE 38th Annual International Conference of the*, pages 259–262. IEEE, 2016. URL http://ieeexplore.ieee.org/abstract/document/7590689/.

[61] Matthew P. Wallen, Sjaan R. Gomersall, Shelley E. Keating, Ulrik Wisløff, and Jeff S. Coombes. Accuracy of heart rate watches: Implications for weight management. *PloS one*, 11(5):e0154420, 2016. URL http://journals.plos.org/plosone/article?id=10.1371/journal.pone.0154420.

[62] Siying Wang, Antje Pohl, Timo Jaeschke, Michael Czaplik, Marcus Köny, Steffen Leonhardt, and Nils Pohl. A novel ultra-wideband 80 GHz FMCW radar system for contactless monitoring of vital signs. In *Engineering in Medicine and Biology Society (EMBC), 2015 37th Annual International Conference of the IEEE*, pages 4978–4981. IEEE, 2015. URL http://ieeexplore.ieee.org/abstract/document/7319509/.

[63] Andrew D. Wiens and Omer T. Inan. A Novel System Identification Technique for Improved Wearable Hemodynamics Assessment. *IEEE Transactions on Biomedical Engineering*, 62(5):1345–1354, May 2015. ISSN 0018-9294, 1558-2531. doi: 10.1109/TBME.2014.2387354. URL http://ieeexplore.ieee.org/document/7001053/.

[64] Andrew D. Wiens, Mozziyar Etemadi, Shuvo Roy, Liviu Klein, and Omer T. Inan. Toward Continuous, Noninvasive Assessment of Ventricular Function and Hemodynamics: Wearable Ballistocardiography. *IEEE Journal of Biomedical and Health Informatics*, 19(4):1435–1442, July 2015. ISSN 2168-2194, 2168-2208. doi: 10.1109/JBHI.2014.2359937. URL http://ieeexplore.ieee.org/document/6907954/.

[65] Zhicheng Yang, Parth H. Pathak, Yunze Zeng, Xixi Liran, and Prasant Mohapatra. Monitoring vital signs using millimeter wave. pages 211–220. ACM Press, 2016. ISBN 978-1-4503-4184-4. doi: 10.1145/2942358.2942381. URL http://dl.acm.org/citation.cfm?doid=2942358.2942381.

[66] Yong-Poh Yu, Ban-Hoe Kwan, Chern-Loon Lim, Siaw-Lang Wong, and P. Raveendran. Video-based heart rate measurement using short-time Fourier transform. In *Intelligent Signal Processing and Communications Systems (ISPACS), 2013 International Symposium on*, pages 704–707. IEEE, 2013. URL http://ieeexplore.ieee.org/abstract/document/6704640/.

[67] Wei Zeng, Qi Zhang, Yimin Zhou, Guoqing Xu, and Guoyuan Liang. Infrared video based non-invasive heart rate measurement. In *Robotics and Biomimetics (ROBIO), 2015 IEEE International Conference on*, pages 1041–1046. IEEE, 2015. URL http://ieeexplore.ieee.org/abstract/document/7418909/.